

**MECHANISMS OF FATIGUE IN
1100-0 AND 2024-T4 ALUMINUM**

J. C. GROSSKREUTZ

G. G. SHAW


FOREWORD

This report was prepared by Midwest Research Institute, 425 Volker Boulevard, Kansas City, Missouri 64110, under USAF Contract No. AF 33(657)-10883. This contract was initiated under Project No. 7353 "Characterization of Solid Phase and Interphase Phenomena in Crystalline Substances," Task No. 735301, "Mechanical Metallurgy." The work was monitored by the Air Force Materials Laboratory, Research and Technology Division, Air Force Systems Command, Wright-Patterson Air Force Base, Ohio, with Mr. K. D. Shimmin, MAMD, acting as Project Engineer.

This report covers work done during the period 1 April 1964 to 31 March 1965. The manuscript was released by the author in March 1965 for publication as an RTD Technical Report.

Dr. J. C. Grosskreutz served as project leader during this research and Mr. Gordon Shaw performed the fatigue testing and electron microscopy. Mr. Sidney Hamilton assisted in preparation and replication of samples.

This technical report has been reviewed and is approved.



W. J. TRAPP
Chief, Strength and Dynamics Branch
Metals and Ceramics Division
Air Force Materials Laboratory

ABSTRACT

The mechanisms of fatigue in notched 1100-0 and 2024-T4 aluminum have been studied by means of optical and electron microscopy. It was found that fatigue cracks nucleated at slip bands on the surface of 1100-0 aluminum in less than 0.5 per cent of total fatigue life. These slip-band fissure cracks grew independently for 65 - 70 per cent of life and then linked rather quickly into a dominant crack which accounted for final failure. The crack growth rates were recorded for both fissure and dominant cracks. On the surface of 2024-T4 aluminum, cracks nucleated in pairs at constituent particle inclusions in less than 5 per cent of total fatigue life. At low stresses, a single crack-pair grew across the notch in about 90 per cent of life and accounted for complete failure as it continued across the sample face. At high stresses, many crack-pairs were nucleated in the notch, some of which linked to form a dominant crack at ~ 50 per cent of life. The difference in crack growth rate dependence on $\sigma\sqrt{l}$, observed for 1100-0 and 2024-T4 aluminum, is discussed in terms of the different dislocation distributions observed at the crack tips. Crack extension in both 1100-0 and 2024-T4 aluminum was observed to occur by a heterogeneous mixture of ripple formation, ductile and cleavage fracture which occurs noncoherently at local regions along the crack front. Some of the consequences of this observation for crack propagation theories are discussed.

Contrails

TABLE OF CONTENTS

	PAGE
I. INTRODUCTION	1
II. EXPERIMENTAL DETAILS	2
A. SAMPLES	2
B. FATIGUE LOADING	4
C. TECHNIQUE FOR OBSERVING CRACK NUCLEATION AND PROPAGATION	5
III. EXPERIMENTAL RESULTS	7
A. 1100-0 ALUMINUM	7
B. 2024-T4 ALUMINUM	15
IV. DISCUSSION OF RESULTS	31
V. CONCLUSIONS	36
REFERENCES	37

Contrails

ILLUSTRATIONS

FIGURE	TITLE	PAGE
1	SAMPLE SHAPES FOR 1100-0 AND 2024-T4 ALUMINUM FATIGUED IN FULLY REVERSED PUSH-PULL LOADING	3
2	SAMPLE PREPARATION FOR ELECTRON MICROSCOPY	6
3	DIRECT FORMVAR REPLICAS (negative) OF NOTCH SURFACE ON 1100-0 ALUMINUM WHICH SHOW FISSURE DEVELOPMENT	8
4	DIRECT FORMVAR REPLICA OF NOTCH CRACK ON 1100-0 ALUMINUM	9
5	OPTICAL MICROGRAPHS SHOWING FISSURE DEVELOPMENT AND LINKAGE TO FORM A DOMINANT CRACK	10
6	CRACK LENGTH, AS OBSERVED ON THE FACE OF 1100-0 ALUMINUM SAMPLES <u>VERSUS</u> NUMBER OF ELAPSED CYCLES	12
7	CRACK GROWTH RATE ON THE FACE OF 1100-0 ALUMINUM SAMPLES <u>VERSUS</u> THE STRESS CONCENTRATION FACTOR $\sigma \sqrt{l}$	13
8	ELECTRON MICROGRAPHS OF TYPICAL FRACTURE SURFACE AREAS ON 1100-0 ALUMINUM	14
9	TRANSMISSION ELECTRON MICROGRAPHS OF 1100-0 ALUMINUM	16
10	ELECTRON MICROGRAPH (surface replica) OF CRACK-PAIR WHICH HAS NUCLEATED AT AN INCLUSION ON 2024-T4 AFTER 5 PER CENT OF TOTAL LIFE TO FAILURE	17
11	OPTICAL MICROGRAPHS SHOWING EARLY CRACK GROWTH IN 2024-T4 ALUMINUM	19
12	OPTICAL MICROGRAPH OF AN INCLUSION CRACK-PAIR ON 2024-T4 ALUMINUM AFTER 5 PER CENT OF TOTAL LIFE AT HIGH STRESS LEVEL	20
13	OPTICAL MICROGRAPH OF LATE STAGE OF CRACK GROWTH ACROSS FACE OF 2024-T4 ALUMINUM	20
14	CRACK LENGTH, OBSERVED IN THE NOTCH AND ON THE FACE OF 2024-T4 ALUMINUM SAMPLES, <u>VERSUS</u> NUMBER OF ELAPSED CYCLES	21

ILLUSTRATIONS (Concluded)

FIGURE	TITLE	PAGE
15	CRACK GROWTH RATE IN THE NOTCH OF 2024-T4 ALUMINUM SAMPLES <u>VERSUS</u> THE STRESS CONCENTRATION FACTOR $\sigma \sqrt{l}$	22
16	ELECTRON MICROGRAPHS OF EARLY CRACK SURFACES ON 2024-T4	23
17	SCHEMATIC REPRESENTATION OF CRACK FRONT IN 2024-T4 FATIGUED AT LOW STRESS (a), AND HIGH STRESS (b)	24
18	ELECTRON MICROGRAPHS OF TYPICAL FRACTURE SURFACE AREA ON 2024-T4 ALUMINUM	26
19	TRANSMISSION ELECTRON MICROGRAPHS OF 2024-T4 ALUMINUM	29
20	SCHEMATIC REPRESENTATION OF HETEROGENEOUS CRACK EXTENSION MECHANISMS	32

Contrails

TABLES

TABLE	TITLE	PAGE
1	NOMINAL COMPOSITION OF ALUMINUM ALLOYS EXPRESSED AS WEIGHT - PER CENT	4
2	STRESS LEVELS AND AVERAGE FATIGUE LIVES FOR 1100-0 AND 2024-T4 ALUMINUM TESTED IN PUSH-PULL	4

I. INTRODUCTION

Fatigue fracture has been customarily considered to be divided into crack initiation and crack propagation stages. Mechanisms have been sought to describe these two stages, and there now exists considerable evidence to show that for pure materials and high purity alloys initiation occurs in surface slip bands and that propagation proceeds through shear (Stage I) and tensile (Stage II) modes (Ref. 1). The mechanisms which govern the fatigue of alloys of commercial purity have not been so clearly demonstrated. Because of the great practical significance of these latter materials, it is desirable that the same sophisticated methods be applied to their study as have been applied to the pure materials. For the present study, we have chosen commercially pure aluminum (99.0 per cent), usually designated as 1100 aluminum, and 2024 aluminum alloy. The first material should allow for comparison of our results with those obtained for pure materials, while the latter should provide the opportunity for understanding fatigue in materials of practical significance.

Our experience of the past several years has shown that fatigue fracture results from a sequence of highly localized events. The important observables in fatigue mechanisms research can be listed as follows:

1. Crack nucleation site
2. Crack nucleation time (fraction of total life)
3. Crack nucleation mechanism (if possible)
4. Crack growth rate
5. Crack growth mechanisms as determined by
 - a. Crack tip studies
 - b. Fracture surface studies

For the earliest possible detection of a crack, it is necessary that observation be made with the highest possible resolution. At the present time, the electron microscope possesses the best available resolution (of the order of 10 \AA). Therefore, the research to be described in this report makes use of techniques developed especially for applying the electron microscope to fatigue research. In addition, optical methods of observation are used to supplement and extend the electron optical measurements. The use of these observational techniques is in keeping with the philosophy that

Contrails

fatigue fracture can best be studied by techniques which are highly selective and capable of distinguishing localized fracture phenomena from the generalized response of a material to cyclic loading, e.g., fatigue hardening.

The experiments to be described in this report have also been designed to shed light on the question, "When does a crack stop initiating and start propagating?". The difficulties inherent in answering this question lie partly in a definition of terms and partly in the resolution of the observational technique. By using the highest resolution available, the latter difficulty is made simply a function of the state of the art. A careful discussion of the proper definition of terms is given in the concluding section of this report.

Notched samples were used in this work for two very important reasons. First, high resolution microscopy would require inordinate amounts of time to search for microcracks unless the area of crack initiation were somehow localized. Second, the study of crack nucleation and growth in a notch is highly practical because nearly all structures of engineering interest are observed to develop fatigue cracks at a stress raiser of some sort, e.g., a fillet or rivet hole.

The research to be described has three objectives: the clarification of fatigue mechanisms in materials of commercial interest; clarification of the transition period between crack initiation and growth; and the description of the initiation and growth of fatigue cracks in a practical geometrical configuration, i.e., a notch. Fatigue mechanisms research of this type is a natural outgrowth of our earlier work which has concentrated on more idealized specimen shapes and high purity materials.

II. EXPERIMENTAL DETAILS

A. Samples

Samples of 1100 aluminum, 1/8 in. thick, and 2024 aluminum, 1/10 in. thick, were prepared from rolled sheet into the shapes shown in Figure 1. Nominal composition limits of the materials are shown in Table 1.

Contrails

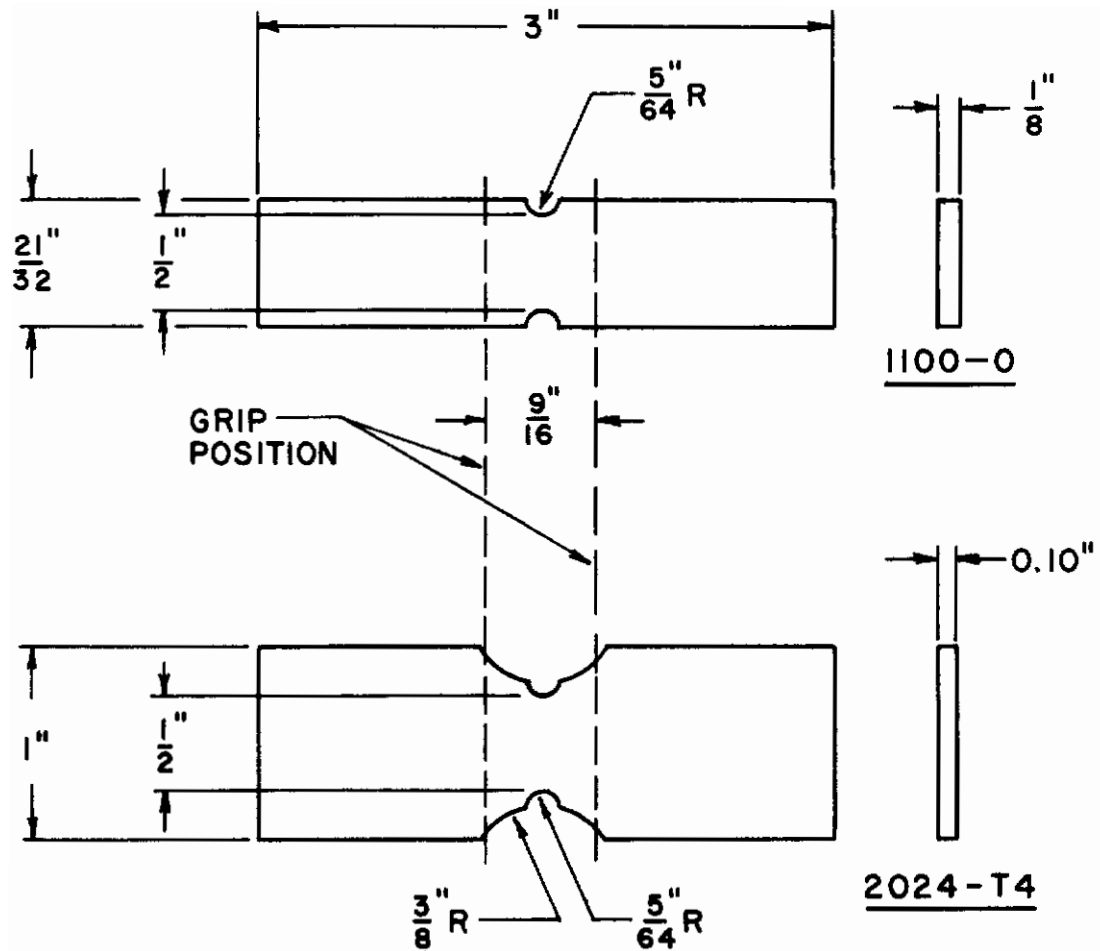


Figure 1 - Sample Shapes For 1100-0 and 2024-T4 Aluminum Fatigued in Fully Reversed Push-Pull Loading

TABLE 1

NOMINAL COMPOSITION OF ALUMINUM ALLOYS
EXPRESSED AS WEIGHT - PER CENT

Alloy	Si	Fe	Cu	Mn	Mg	Zn
1100	1.0		0.2	0.05	-	0.10
2024	0.5	0.5	4.5	0.6	1.5	0.25

After fabrication, the 1100 aluminum samples were heat-treated to the O condition by annealing at 340°C for 1 hr., and the 2024 aluminum was heat-treated to the T4 condition by solution heat treatment at 500°C for 1 hr., quenching into cold water and aging at room temperature for four days. All samples were electropolished briefly in a solution of 20 per cent perchloric acid and 80 per cent ethanol.

B. Fatigue Loading

All samples were run in fully reversed push-pull under constant load in a Sontag SF-U-1 fatigue machine. Loads were normally chosen to give fatigue lives of the order of 2 - 3 million cycles. Also, 2024-T4 aluminum was investigated at a higher stress level for which the fatigue life was of the order of 10^5 cycles. Corresponding stress levels and fatigue lives are listed in Table 2.

TABLE 2

STRESS LEVELS AND AVERAGE FATIGUE LIVES FOR 1100-O AND
2024-T4 ALUMINUM TESTED IN PUSH-PULL

Material	Nominal Stress	Average Fatigue Life
1100-O	± 4,160 psi	2.3×10^6 cycles
2024-T4	± 18,000 psi	9.2×10^4 cycles
2024-T4	± 13,600 psi	2.34×10^6 cycles

C. Technique for Observing Crack Nucleation and Propagation

Samples were loaded into the grips of the Sontag fatigue machine and cycling begun at a predetermined load level. At selected intervals, the test was stopped and surface replicas were made of the notches and faces of the sample without moving it from the grips. These replicas were made with either silicon rubber (Ref. 2) or Faxfilm. Some samples were replicated every 100,000 cycles so that up to 60 replicas were accumulated per sample. These replicas were viewed directly with an optical microscope and the notch was scanned for evidence of fatigue cracks at various stages of life. (Because of the re-entrant shape of the silicon rubber replicas, it was found easier to prepare secondary polystyrene replicas for the optical examination.) The measurement of crack length versus number of cycles was made directly from these replicas.

The silicon rubber and Faxfilm replicas were also used for electron microscope examination of the surface. Secondary formvar replicas were stripped from the primary Faxfilm or silicone rubber molds, shadowed with platinum-palladium, and backed with carbon. These secondary replicas were then washed in ethylene dichloride and examined in the electron microscope. The resolution which was obtained with these two stage replicas was not always as great as desired. Therefore, in certain cases of interest, the aluminum samples were completely removed from the Sontag machine and the notches replicated directly with formvar.

Cycling was usually stopped when a dominant crack had progressed about one-third to one-half the distance across the face of the sample. The specimen was then pulled apart by means of the preload motor on the Sontag machine, thereby exposing the fatigue fracture surface for further studies. This fracture surface, as well as the notch surface adjacent to the point of crack nucleation, was replicated directly with formvar, shadowed, and examined in the electron microscope. The technique is illustrated in Figure 2(a). Shadowing was carried out at 45 degrees to the fracture surface and in the direction of crack advance.

The condition of the material adjacent to the fracture surface or near the tip of the propagating crack was viewed directly with an electron microscope by use of a unique sample preparation technique developed especially for this research. The technique provides strain-free foils suitable for electron transmission (thickness, 2,000 - 5,000 Å) as near to the crack as is desired. As illustrated in Figure 2(b), sections were cut either parallel to the fracture surface (A), or perpendicular to the crack at its tip (B). For observation adjacent to the crack, chemical thinning was begun at the surface farthest removed from the crack and continued until perforation occurred at the fracture surface. The fracture surface was protected by an acid-resistant coating. Observation at various distances from the crack

Contrails

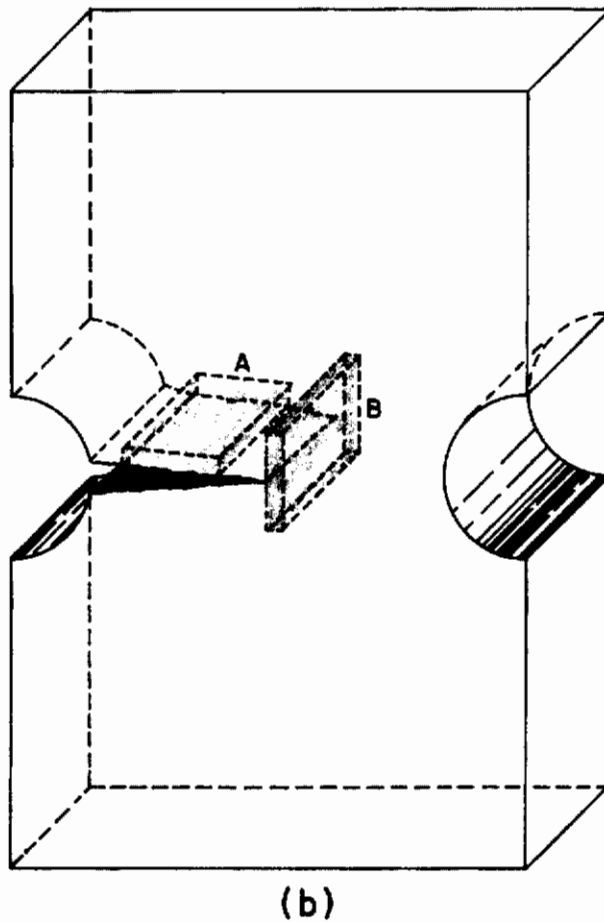
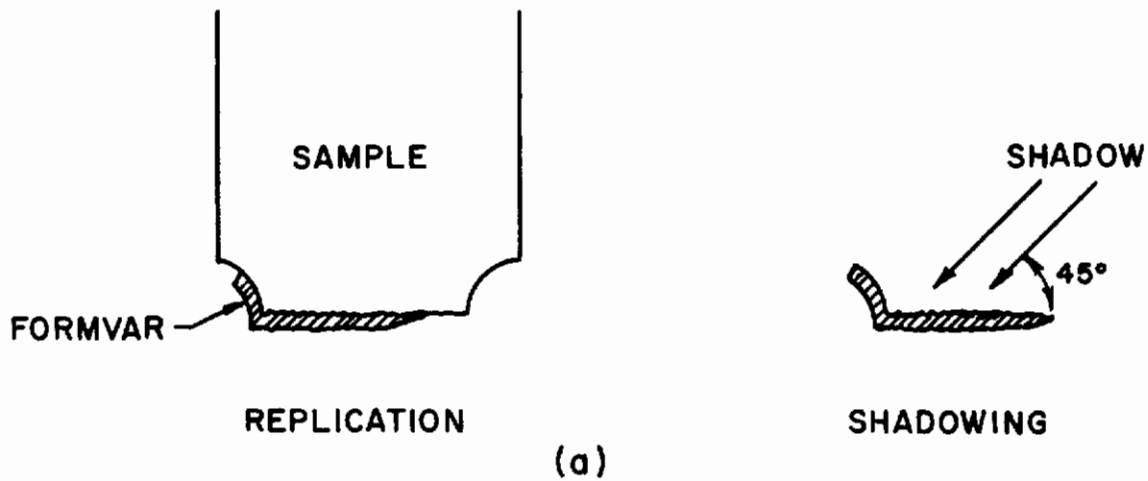


Figure 2 - Sample Preparation For Electron Microscopy. (a) Schematic drawing showing techniques for replication of fracture surface and adjacent notch surface for electron microscope observation; (b) Schematic drawing showing position of sections cut for transmission electron microscopy. Section A includes plastic zone adjacent to crack; Section B contains plastic zone at crack tip.

Contrails

was achieved by first electropolishing the desired amount from the fracture surface before beginning the thinning process from the rear. The section (B) could also be cut some distance ahead of the crack for examination of less severely strained material.

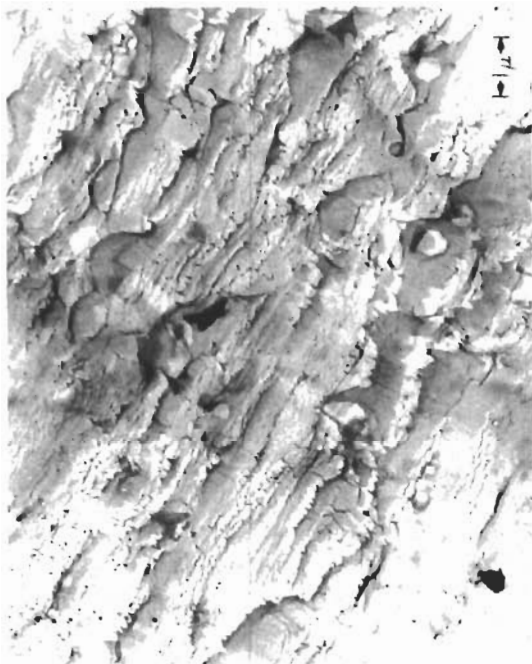
III. EXPERIMENTAL RESULTS

A total of 15 samples of 1100-0 aluminum and 10 samples of 2024-T4 aluminum were run to various stages of fatigue and replicated for observation.

A. 1100-0 Aluminum

1. Crack nucleation: Observations were made on four different samples which were carried through to final fracture. Slip bands were observed to form in favorably oriented grains as early as 0.5 per cent of total life to fracture. These slip bands developed independently into deep fissures as cycling progressed. The sequence shown in Figure 3 was taken from direct (negative) formvar replicas of the notch surface. At 15,000 cycles (Figure 3(a)) the slip bands were still quite shallow, but by 100,000 cycles (Figure 3(b)) they had begun to deepen noticeably. The jagged or serrated edge at the bottom of the fissures is an artifact of the replication and occurred as the replica was stripped from the notch surface and the formvar which filled the fissures pulled loose. At 300,000 and 500,000 cycles (Figures 3(c) and 3(d)) the fissures were deeper still as evidenced by the lengthening shadows cast by the replicating material which penetrated into them. From these and other photographs, the rate at which these fissures deepen could be calculated. We obtain a figure, 2×10^{-2} Å/cycle, which is an average from the depth measurements made at different stages of fissure development. Because the extension per cycle is much less than an atomic dimension in aluminum, we must conclude either that a fissure does not grow on every stress cycle, or that growth occurs only along a limited length of the fissure on each cycle.

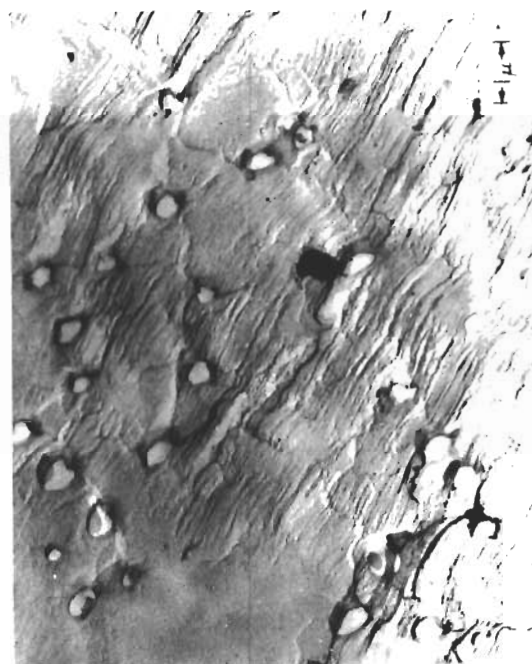
This independent fissure growth continued for $1.5 - 1.8 \times 10^6$ cycles out of a total life of 2.3×10^6 cycles. At that time the favorably oriented fissures linked up into a single dominant crack in a period of less than 100,000 cycles. Figure 4 is a direct formvar replica taken at the tip of a notch crack which is in the process of linking up. Other well developed fissures can be seen on either side of the dominant crack. The total sequence is shown at optical magnification in Figure 5. The curvature of the notch surface accounts for the limited field of view which is in-focus on these pictures. Complete link-up had not yet occurred in Figure 5(c), but 100,000 cycles later (Figure 5(d)) the process had been completed.



(a) 15,000 ~



(b) 100,000 ~



(c) 300,000 ~



(d) 500,000 ~

Figure 3 - Direct Formvar Replicas (negative) of Notch Surface on 1100-0 Aluminum Which Show Fissure Development. Direction of shadow is along tensile axis in each case.

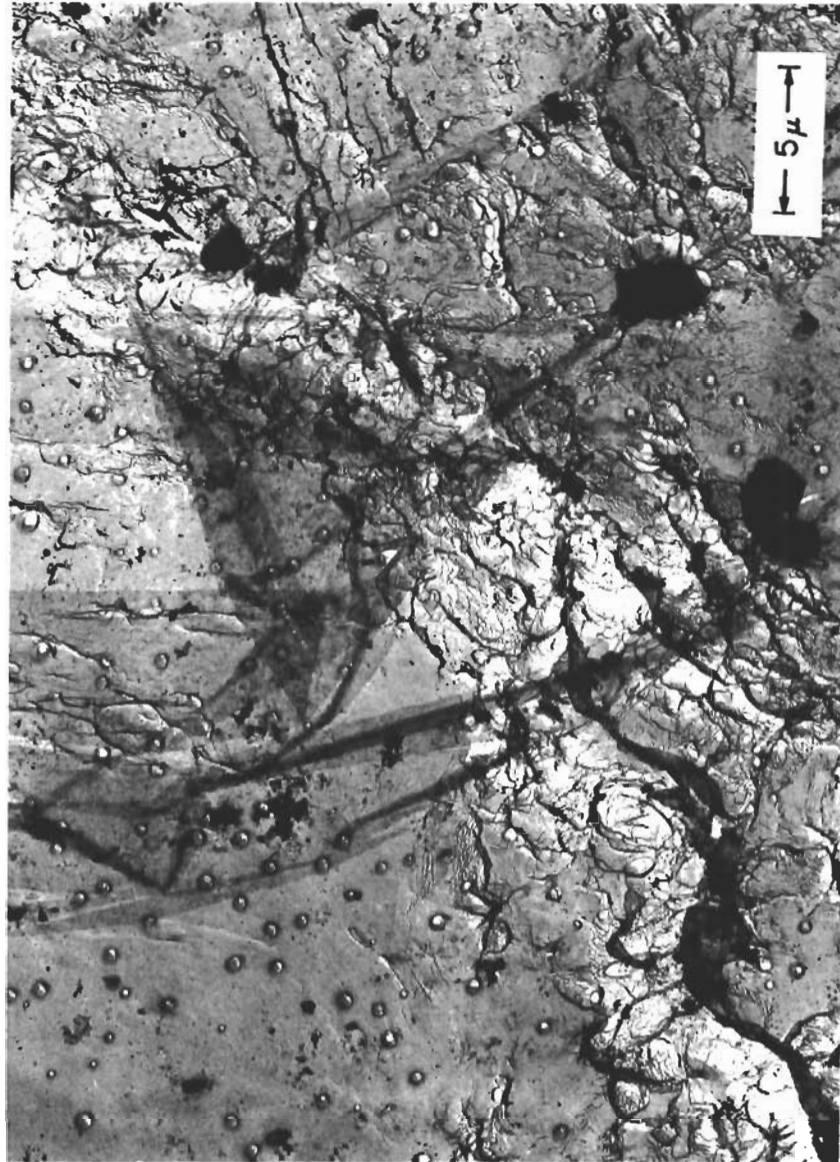
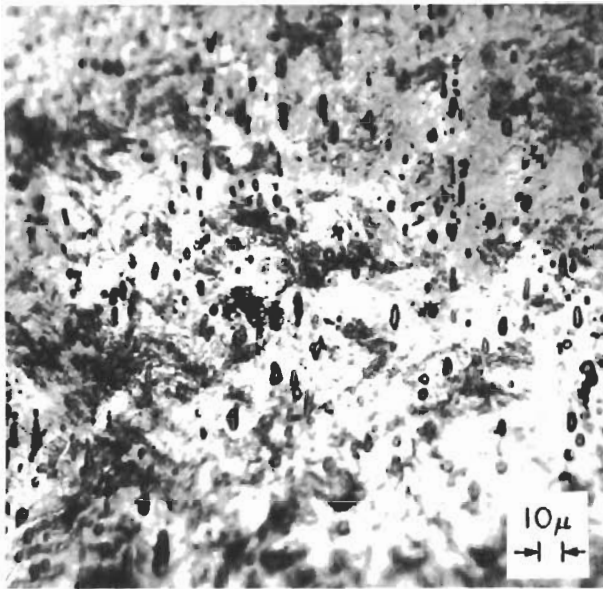
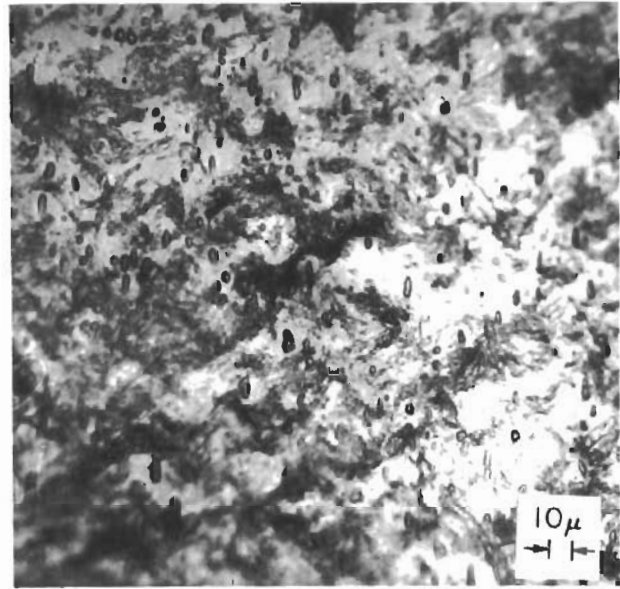


Figure 4 - Direct Formvar Replica of Notch Crack on 1100-O Aluminum.
This crack is in the fissure-linkage stage.
Crack-tip at upper right.

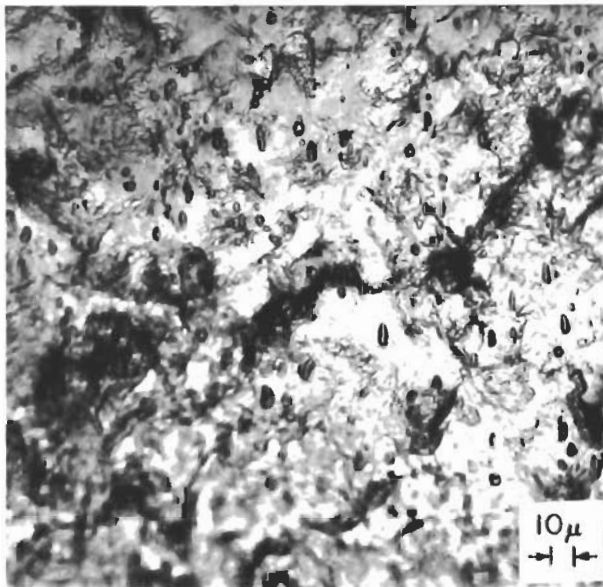
Contrails



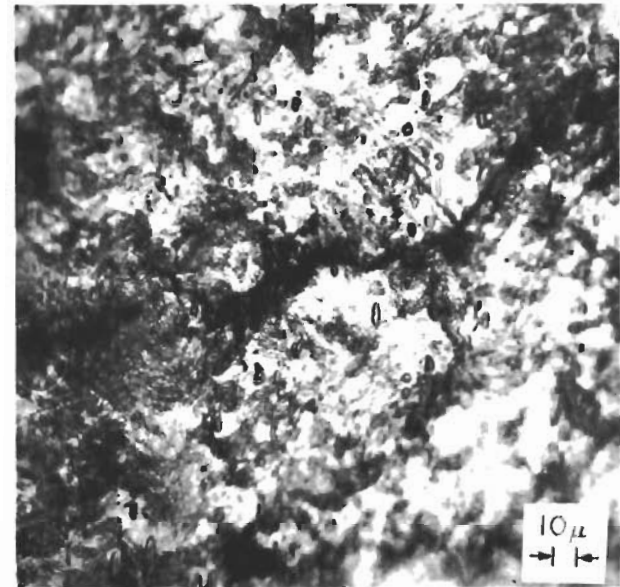
(a) 100,000 ~



(b) 500,000 ~



(c) 1,700,000 ~



(d) 1,800,000 ~

Figure 5 - Optical Micrographs Showing Fissure Development and Linkage to Form a Dominant Crack. Same field of view in all stages; tensile axis vertical.

Contrails

The crack nucleation site in 1100-0 aluminum is obviously surface slip bands. If we define nucleation time as the time to develop a dominant fatigue crack, then nearly 70 per cent of total life is necessary. If, on the other hand, we define nucleation time as the time to nucleate any one microcrack, then this time is less than 1 per cent of total life.

2. Crack growth: For purposes of data presentation at this point, we shall define the beginning of crack growth in 1100-0 aluminum as the time of appearance of a single dominant crack. As reported above, slip-band fissures link into a single crack at approximately 65 - 70 per cent of life. This crack was observed to propagate out of the notch immediately and then grow across the face of the sample. If crack length is defined as the distance separating the crack front from the notch surface (measured in x-direction, Figure 17, p. 24), the total crack length at the time growth begins on the face of the sample is probably not over 3 - 5 microns. This figure is obtained by multiplying the observed rate of fissure deepening by the total number of cycles necessary to produce a single dominant crack. Subsequent crack length measurements, as a function of total cycles, were obtained from the face of several samples. These data are plotted in Figure 6.

It is customary (Ref. 3) to plot the slope of the curves in Figure 6 versus a stress intensity factor, $\sigma\sqrt{l}$, where σ is the net section stress and l is the crack length. Figure 7 shows that the data from sample 6 plots with a slope of 2, while that from sample 14 plots with a slope of approximately 3/4. This difference in behavior is due to the fact that the net section stresses in sample 6 were always below the yield stress (5,000 psi), while those in sample 14 rose above the yield stress rather early in the crack life. These data, therefore, support the following crack-growth power law relations:

$$\frac{dl}{dn} = C(\sigma\sqrt{l})^2 ; \sigma < \sigma_y$$

$$\frac{dl}{dn} = C(\sigma\sqrt{l})^{3/4} ; \sigma > \sigma_y .$$

A large number of fracture surface replicas were made and examined in the electron microscope. Figure 8 shows representative examples of typical areas. Fine growth striations are shown in Figure 8(a) adjacent to an area containing many rough facets. The spacing of the striations is approximately 350 Å which indicates a crack growth rate of 3.5×10^{-6} cm/cycle, which is somewhat larger than the largest growth rate observed on the surface of sample 14 (Figure 7).

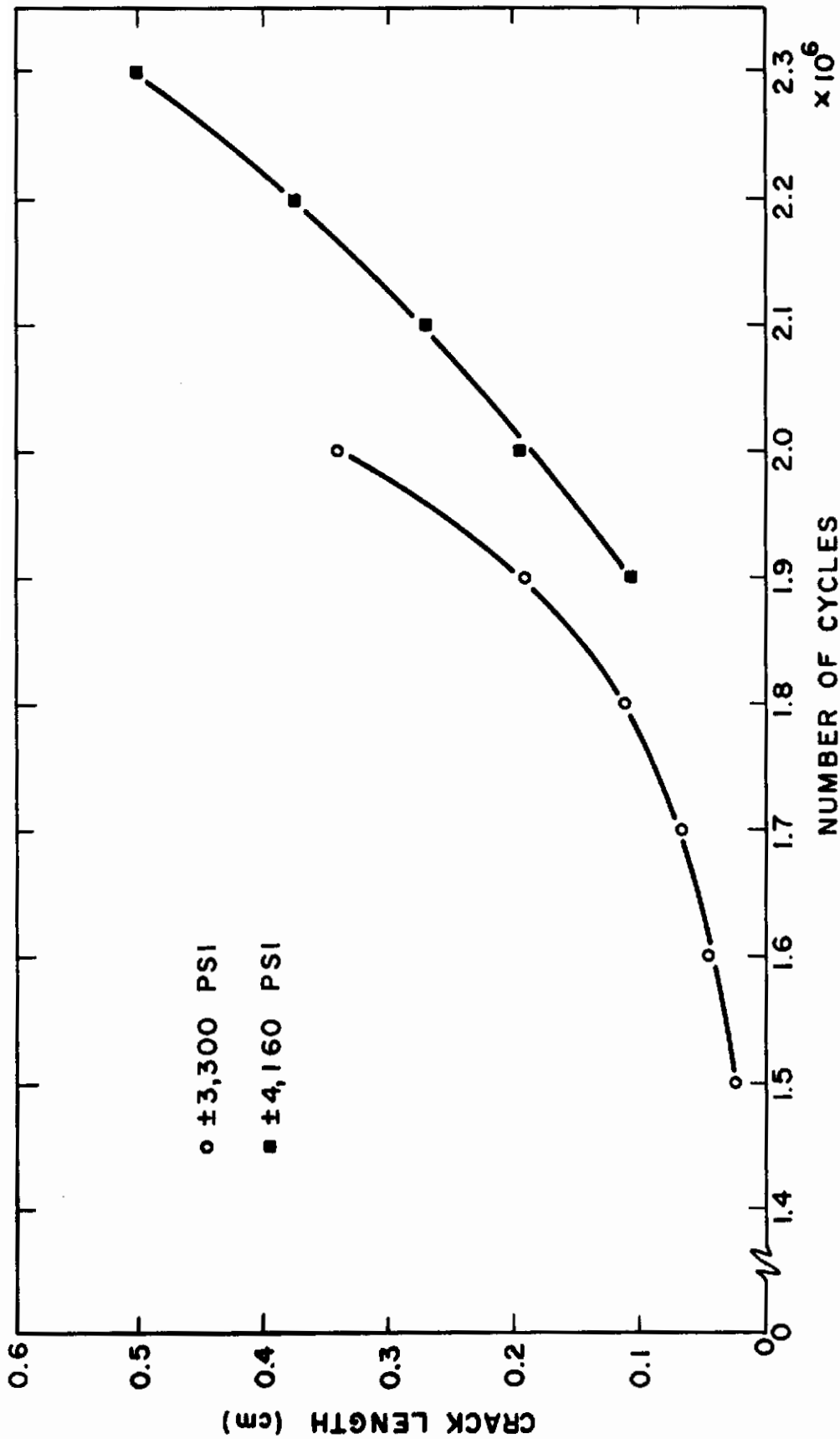


Figure 6 - Crack Length, as Observed on the Face of 1100-0 Aluminum Samples versus Number of Elapsed Cycles

Contrails

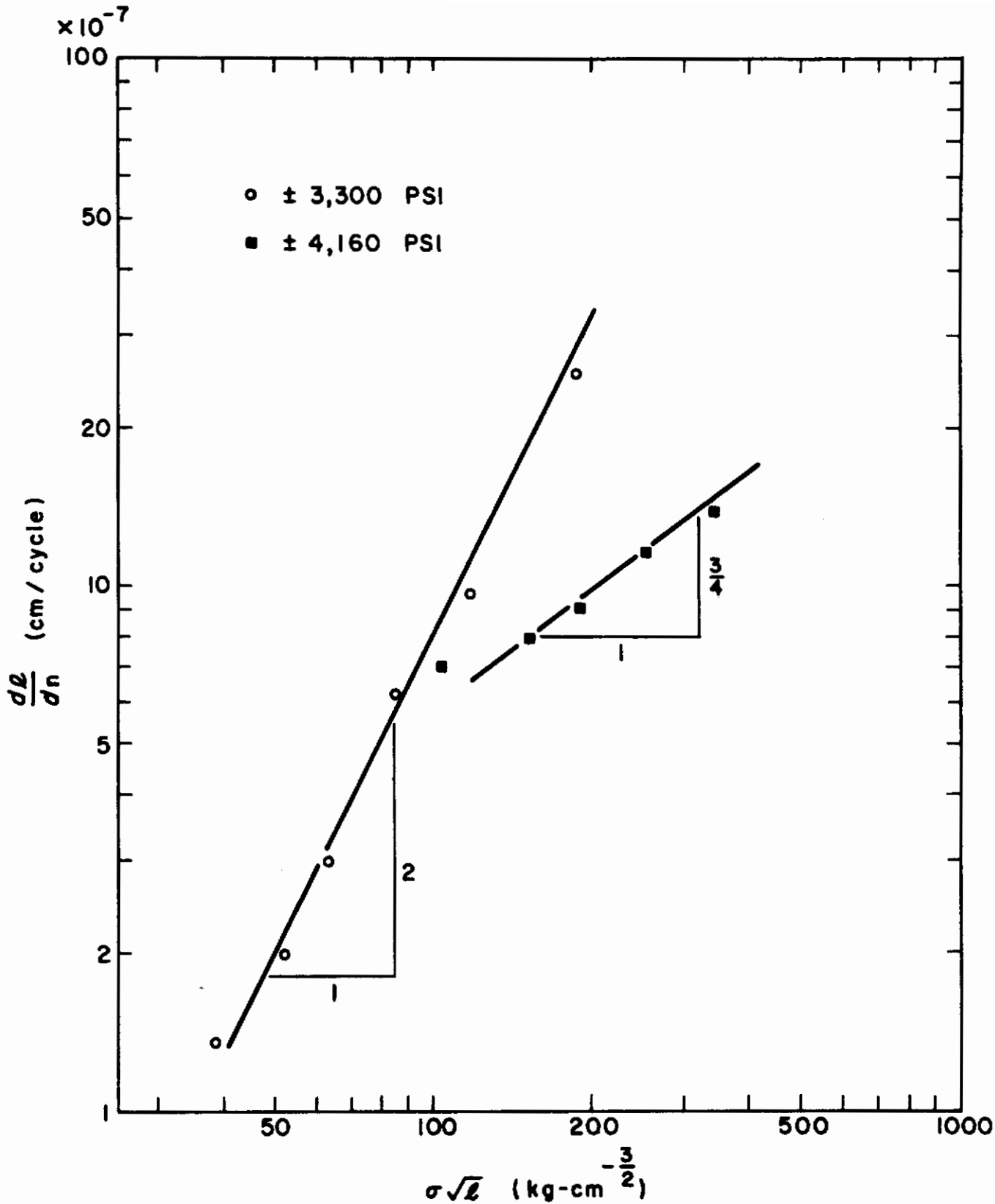
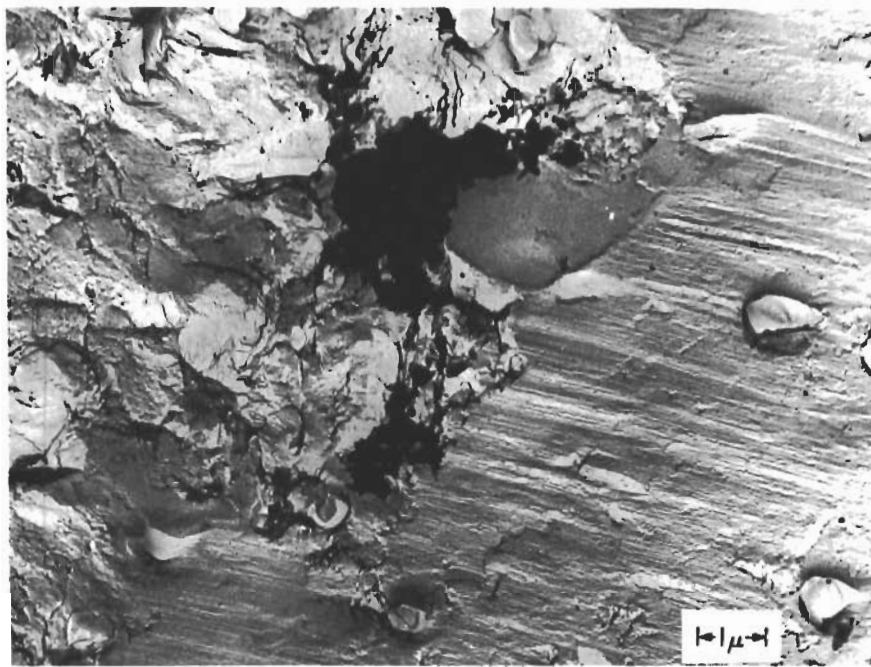
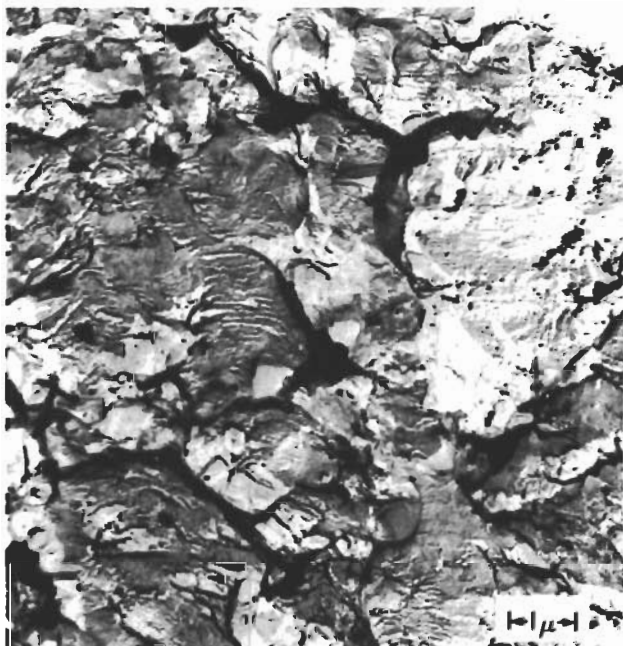


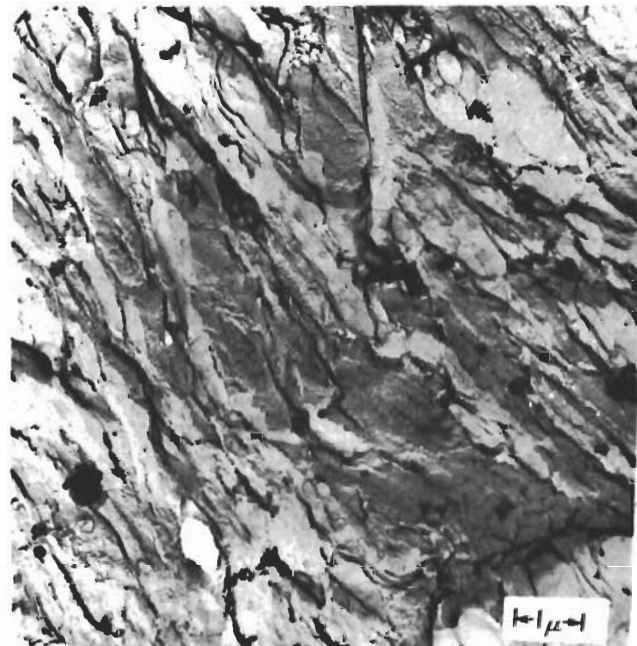
Figure 7 - Crack Growth Rate on the Face of 1100-O Aluminum Samples versus the Stress Intensity Factor $\sigma\sqrt{l}$.



(a)



(b)



(c)

Figure 8 - Electron Micrographs of Typical Fracture Surface Areas on 1100-0 Aluminum.
(a) Fine striations (ripples) adjacent to ductile fracture area; (b) Continuous growth striations across many facets; (c) "River pattern".
Direction of crack growth is nearly vertical in all cases (x-direction).

Contrails

This result infers that propagation does not occur at all points along the crack front on every cycle of stress. This conclusion is supported by noting in Figure 8(a) that the crack front is by no means continuous and that the mechanism of crack growth can change sharply along the crack front. The left-hand area in Figure 8(a) appears to have fractured by a ductile tearing mechanism. On the other hand, Figure 8(b) illustrates a many faceted surface which shows evidence of a fairly continuous crack front. Growth striations can be traced across nearly the entire field of view. Figure 8(c) shows yet a different pattern in which growth striations are almost completely absent and a "river pattern" exists nearly parallel to the direction of crack propagation. Such markings are sometimes found on cleavage fracture surfaces.

A considerable amount of "debris" was pulled from the fracture surface as the plastic replicas were stripped. Examination of this debris with electron diffraction techniques showed that it consisted of aluminum and aluminum oxide particles. These particles are clearly the result of repeated scrubbing of the fracture surfaces as cycling progresses.

Transmission electron microscope studies were carried out on sections cut adjacent to the fracture surface, several thousand microns ahead of the crack tip, and from an uncycled sample. Figure 9(a) shows a typical area in an uncycled control sample. A few dislocations can be seen clustered about impurity particles. These particles occupy a volume fraction of 1.2 per cent in this material. Figure 9(b) shows the dislocation configuration 6 microns from the fracture surface (position A, Figure 2(b)). Well defined subgrains are visible and many impurity particles can be seen in the cell walls. These particles probably serve as nucleation sites for the boundaries. Dense dislocation tangles can also be observed within the cell. The facets observed on fracture surface replicas (Figure 8(b)) are the same size as the cells observed in transmission and undoubtedly are related to fracture along the cell boundaries (Ref. 4). The dislocation distribution 2,500 microns ahead of the crack is illustrated in Figure 9(c). Dislocation tangles and loops are present, a configuration associated with low-strain cycling (Ref. 5). No internal voids were observed in 1100-0 aluminum after cyclic stressing.

B. 2024-T4 Aluminum

1. Crack nucleation: Observations were made on three different samples run to failure at a low stress level, \pm 13,600 psi, and on two samples run to failure at a high stress level, \pm 18,000 psi (see Table 2 for mean lives). Microcracks were observed to nucleate on the surface at constituent particle inclusions. At the low stress level, cracks were first observed optically at about 10 per cent of the total life, while at the electron optical level, isolated surface microcracks could be found as early as 5 per cent of total life. Figure 10 illustrates such a crack.

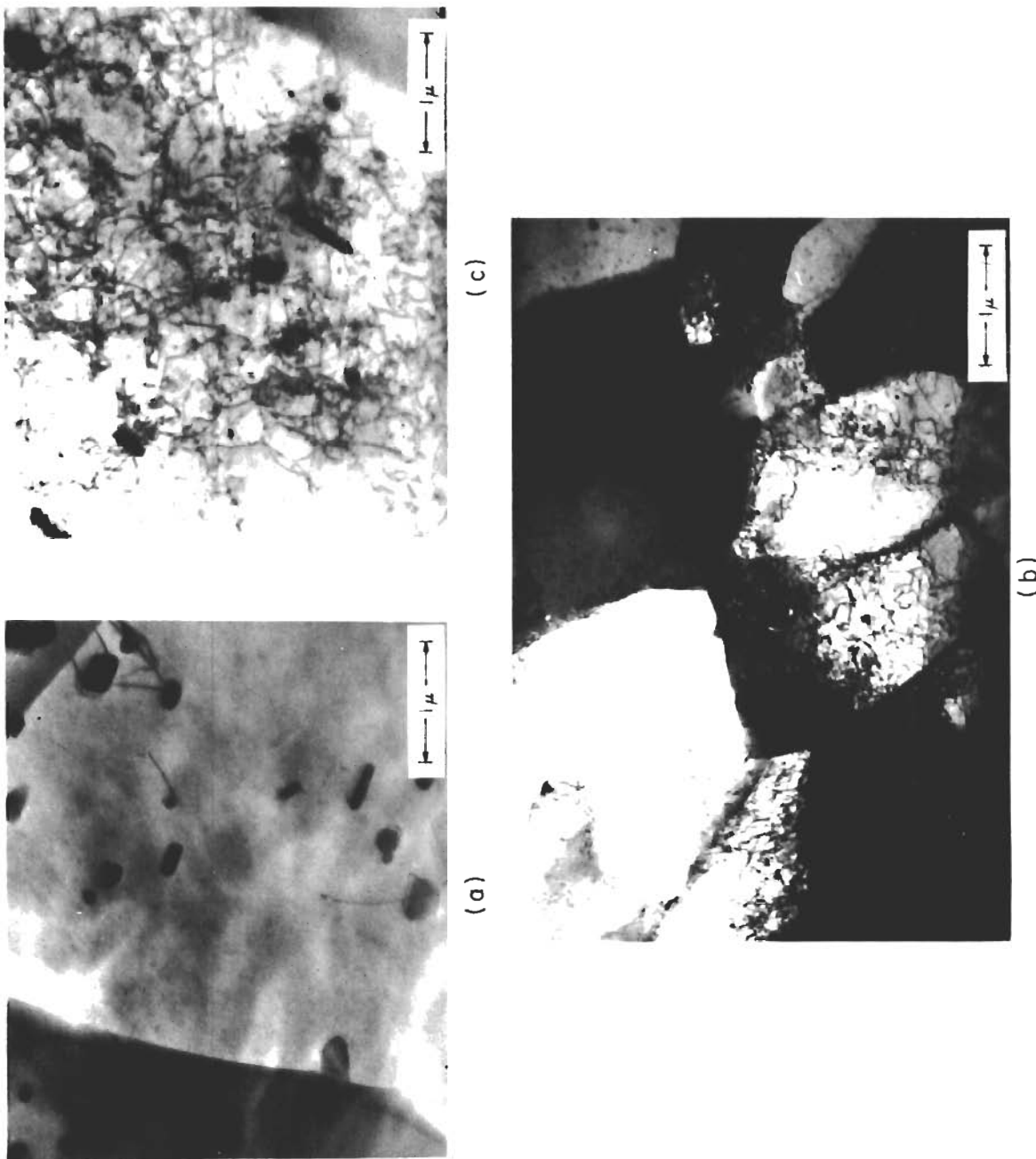


Figure 9 - Transmission Electron Micrographs of 1100-0 Aluminum. (a) Control (uncycled); (b) 6 Microns from fracture surface; (c) 2,500 Microns ahead of crack-tip.

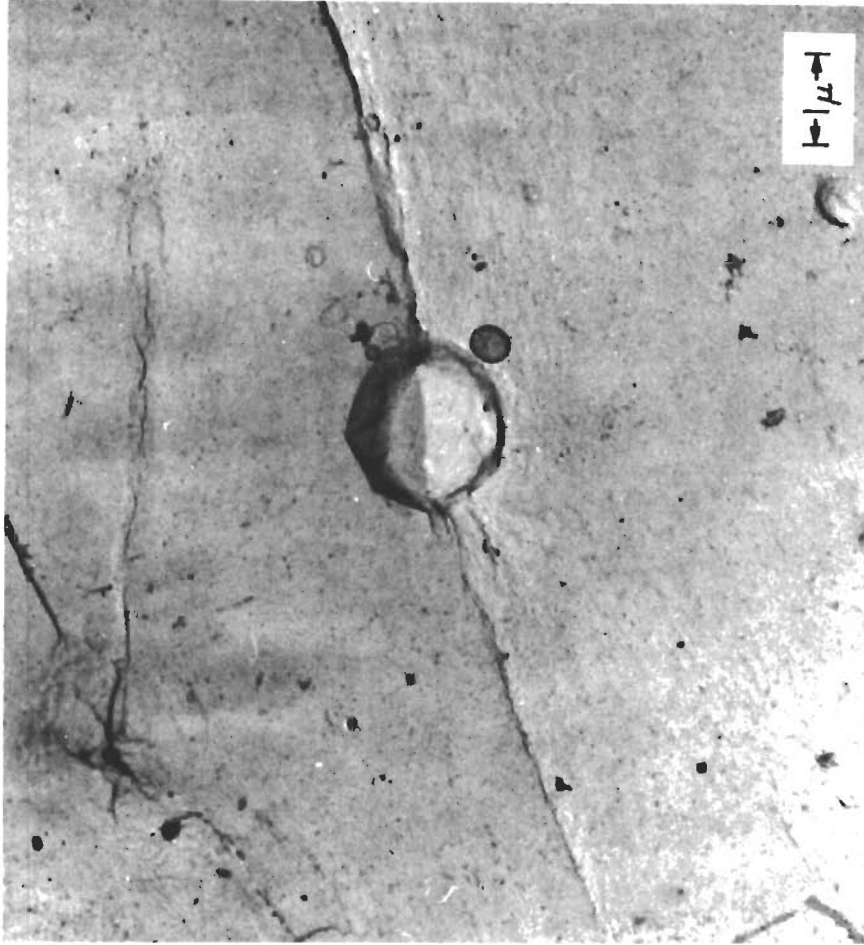


Figure 10 - Electron Micrograph (surface replica) of Crack-Pair Which
Has Nucleated at an Inclusion on 2024-T4 After 5 Per
Cent of Total Life to Failure. \pm 13,600 psi.

Contrails

In all cases observed in 2024-T4 aluminum, cracks nucleated in pairs on opposite sides of the inclusion. At the low stress level, the main fracture crack resulted from continuous growth of one such pair of cracks. However, replicas taken of the notch surface adjacent to the dominant crack showed that other crack pairs had nucleated at other inclusions, but that they did not propagate sufficiently to affect the final fatigue fracture. At the higher stress level, electron micrographs taken at 5 per cent of total life showed many crack pairs which had nucleated at inclusions and linked to other such pairs.

To determine whether these crack pairs were present in the as-received material, surface replicas were taken from the notch of unstrained samples and examined in the electron microscope. No positive identification of actual cracks could be made. Several images were found which could be identified either as microcracks, or as artifacts formed during stripping the plastic replica from the sample surface. Further study of these replicas is planned for the future.

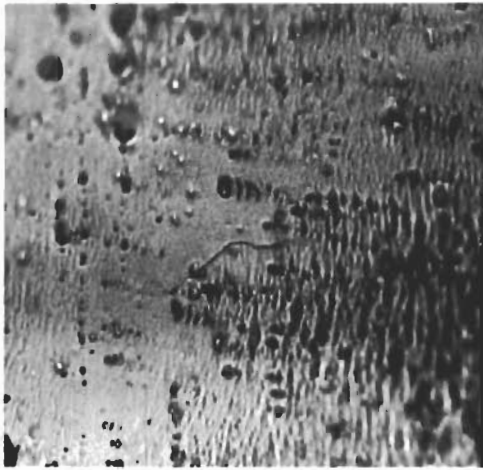
2. Crack growth: At low stress levels, a single crack pair grows to fill the entire notch. Part of this development is shown in the optical sequence of Figure 11. On this particular sample, the crack extended completely across the notch by 3.4×10^6 cycles. The crack then began to grow across the face of the sample and complete failure occurred at 3.84×10^6 cycles.

At the high stress level, as many as 12 different cracks were observed to attain lengths of several hundred microns before a few favorably oriented ones linked to fill the notch. The nucleation of one such crack after 5 per cent of life is shown in Figure 12. Later, when the crack had begun to propagate across the face of the sample, definite indications of plastic deformation (slip) near the crack could be observed (Figure 13). No indication of plastic deformation was ever observed on the notch surface of 2024 aluminum, even at electron optical levels.

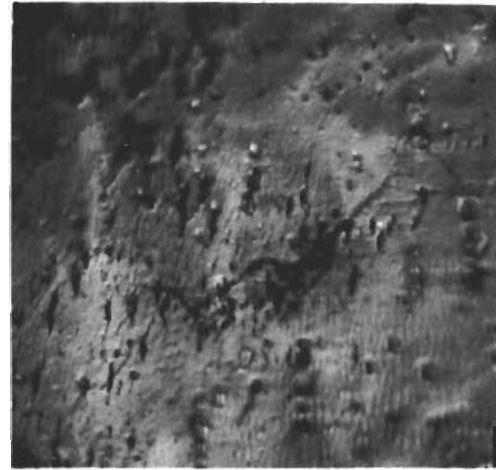
The growth rate of the dominant low-stress crack and one of the high-stress cracks across the notch face was obtained from optical examination of the replicas. The results are shown in Figures 14 and 15. In both cases the net section stress remained below the yield stress and the plots of $\frac{dl}{dn}$ versus $\sigma \sqrt{l}$ yield a slope of 4 for both the low and high stress levels. Thus, the power law relationship for 2024-T4 aluminum is

$$\frac{dl}{dn} = C(\sigma \sqrt{l})^4$$

Contrails

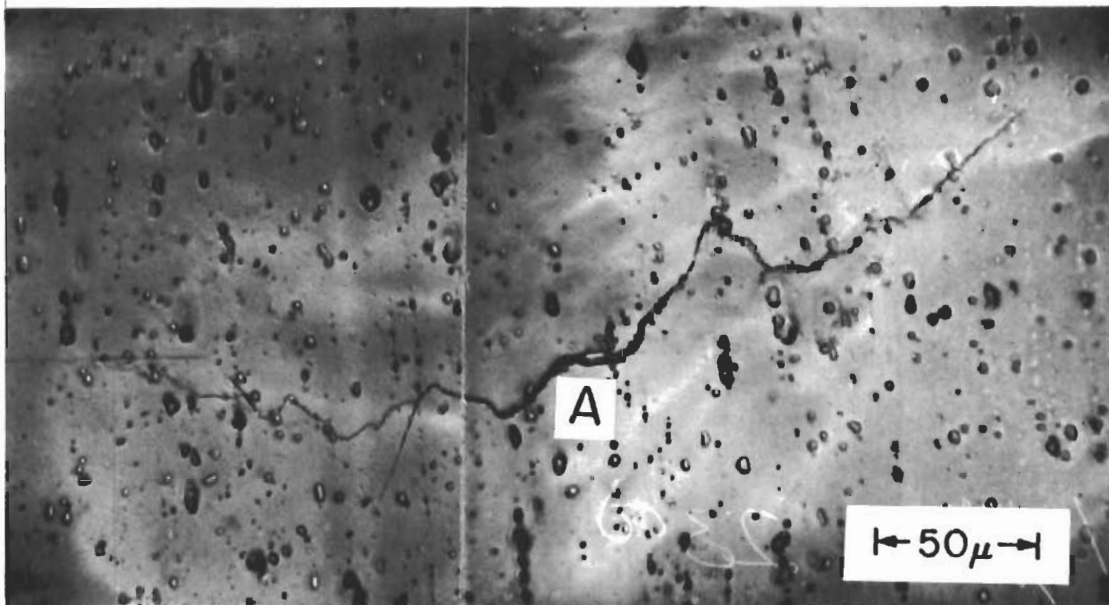


(a) 500,000~



(b) 1,800,000~

←50 μ →



(c) 2,300,000~

Figure 11 - Optical Micrographs Showing Early Crack Growth in 2024-T4 Aluminum. Original nucleus is shown at A in (c).
 $\pm 13,600$ psi.

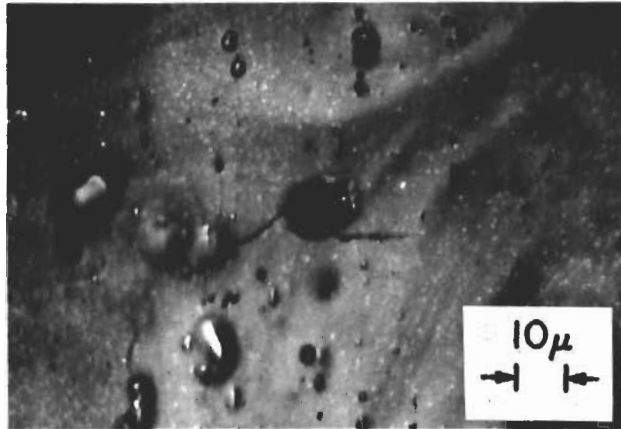


Figure 12 - Optical Micrograph of an Inclusion Crack-Pair on 2024-T4 Aluminum After 5 Per Cent of Total Life at High Stress Level. \pm 18,000 psi.

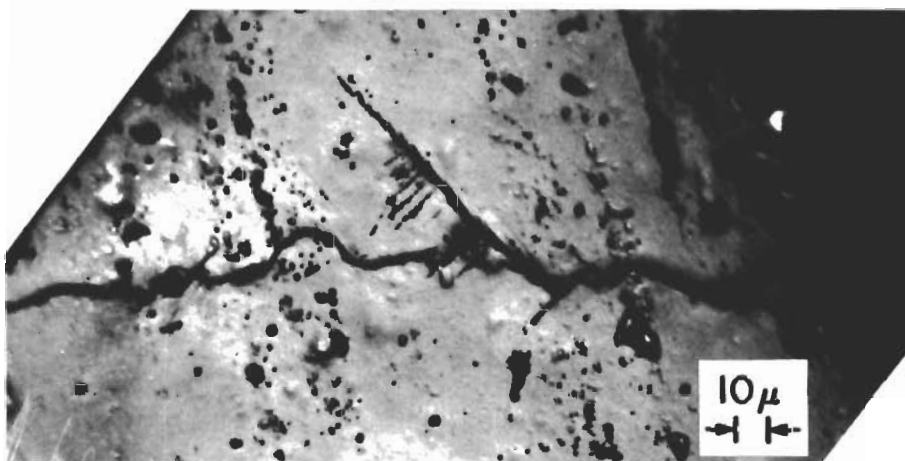


Figure 13 - Optical Micrograph of Late Stage of Crack Growth Across Face of 2024-T4 Aluminum. \pm 18,000 psi. Growth occurred from right to left.

Contrails

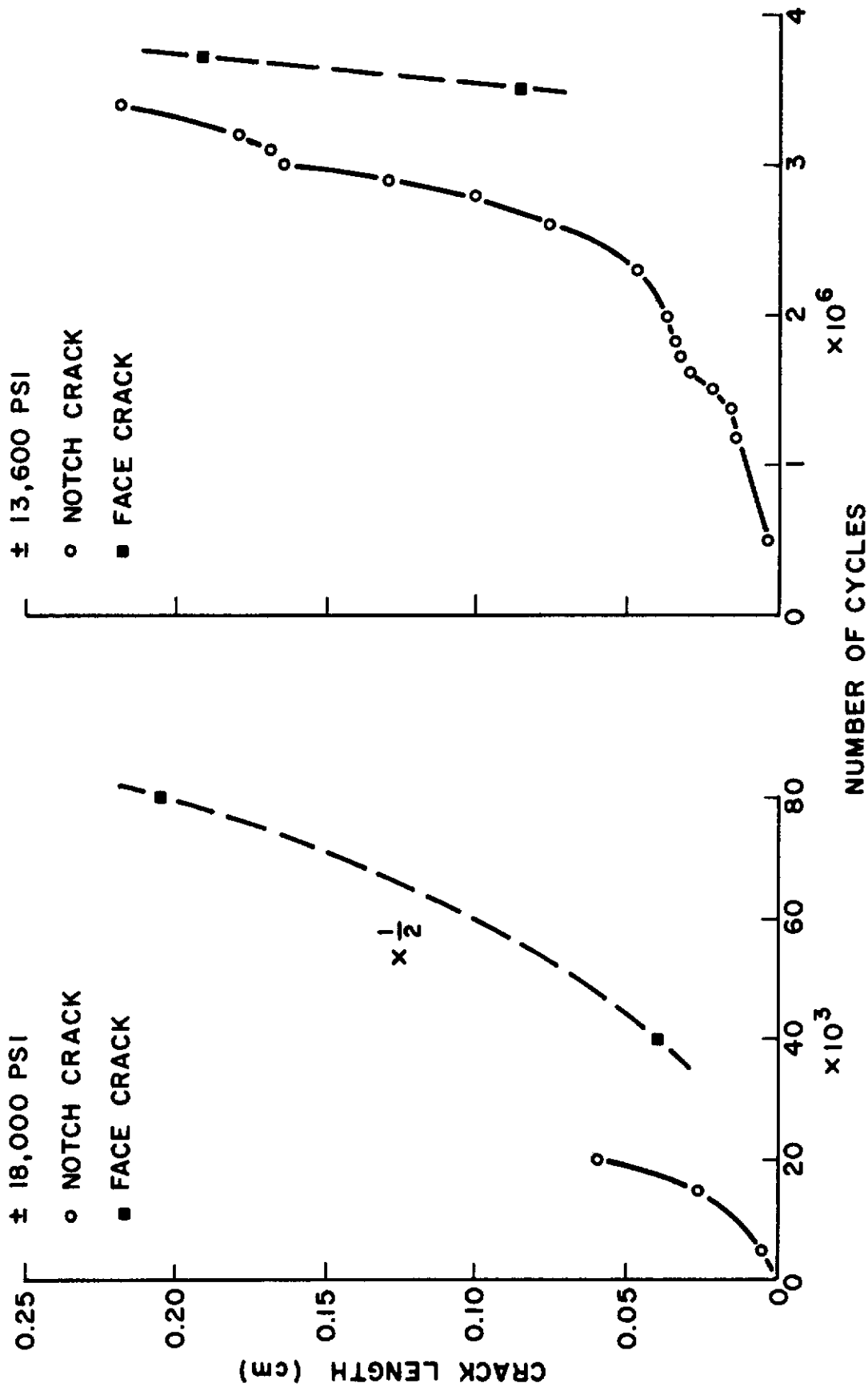


Figure 14 - Crack Length, Observed in the Notch and on the Face of 2024-T4 Aluminum Samples, versus Number of Elapsed Cycles. Notch crack length measured in y-direction (Figure 17) and face crack measured in x-direction.

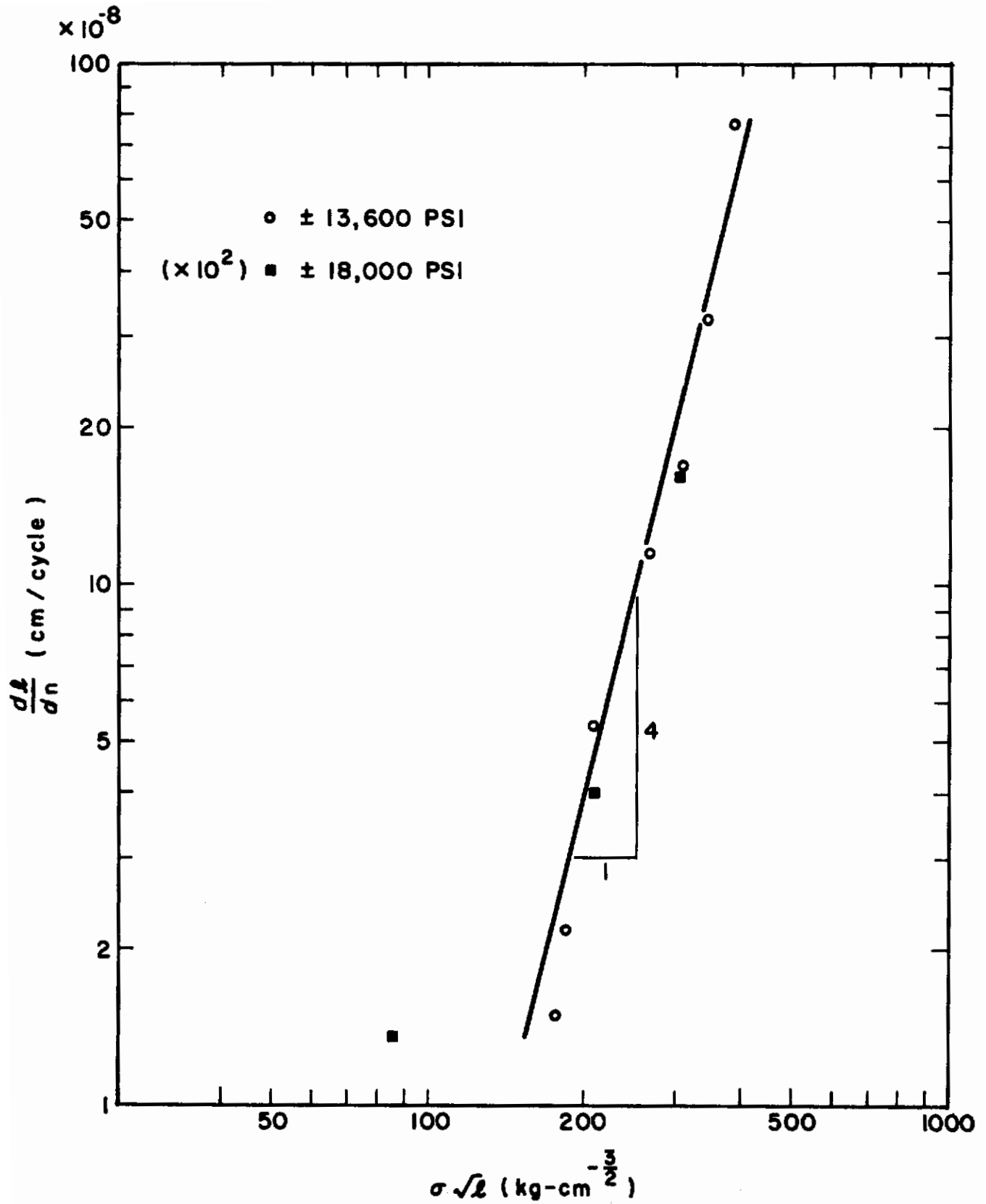
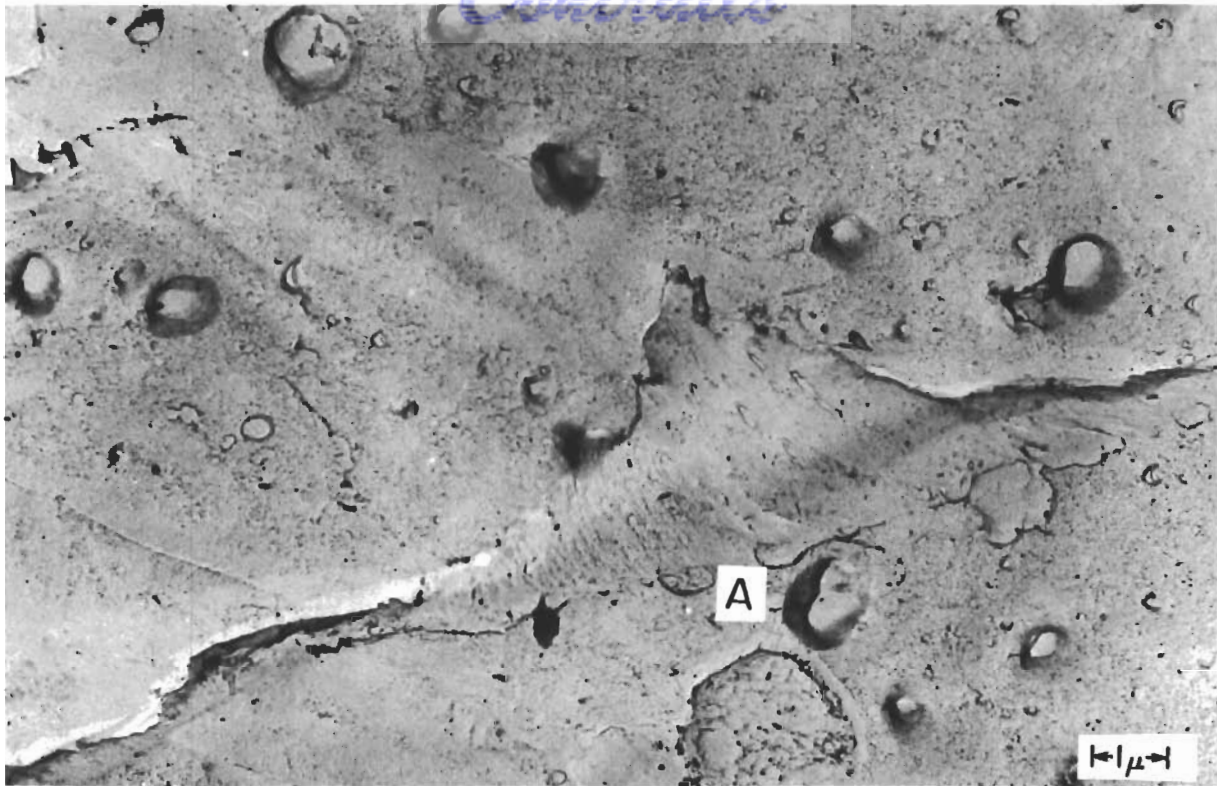
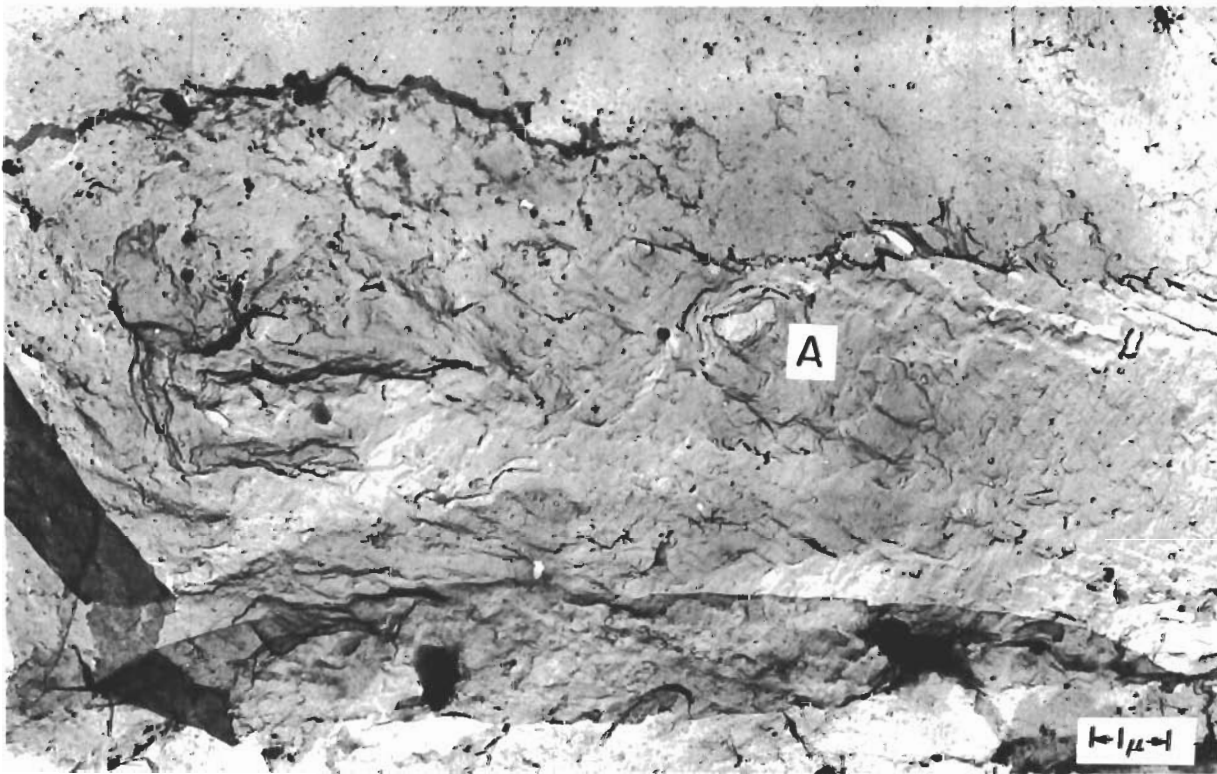


Figure 15 - Crack Growth Rate in the Notch of 2024-T4 Aluminum Samples versus the Stress Intensity Factor $\sigma \sqrt{l}$. Slopes as shown.



(a)



(b)

Figure 16 - Electron Micrographs of Early Crack Surfaces on 2024-T4. (a) After 16,000 cycles at high stress, $\pm 18,000$ psi. Possible nucleating inclusion at A. (b) Interface between notch surface and fracture surface (lower two-thirds of photograph) formed at low stress, $\pm 13,800$ psi. Nucleating inclusion at A.

Contrails

Because crack growth across the face of the sample occupied only about 10 per cent of the total life, reliable growth rate data were not obtained for this stage.

Replicas of the notch surface which were taken during the early stages of microcrack growth show the details of the fracture surface produced during that period. Figure 16(a) is an unusual micrograph which displays a negative replica of a rather deep microcrack in the early stages of growth during high stress fatigue. Faint growth striations can be seen on the left-hand side of the crack face. The sense of the striations indicates lateral growth. The inclusion from which the crack probably started is indicated at A. The nature of the fracture surface during early crack growth was also studied by replication of the fracture surface adjacent to the notch as shown in Figure 2(a). In most cases, the boundary between the notch and the beginning of fracture breaks up during washing of the formvar replica prior to observation. The only example of a continuous replica which we obtained at this interface is shown in Figure 16(b). The nucleating inclusion in this case may well have been the one marked at A. Growth striations are not clearly evident on this surface. Considering the manner in which cracks are observed to nucleate and propagate across the notch surface, the general nature of the dominant crack front in 2024-T4 must be as illustrated in Figure 17. It is clear that significantly different crack growth laws might result depending upon whether the propagation vector was taken in the x or y direction.

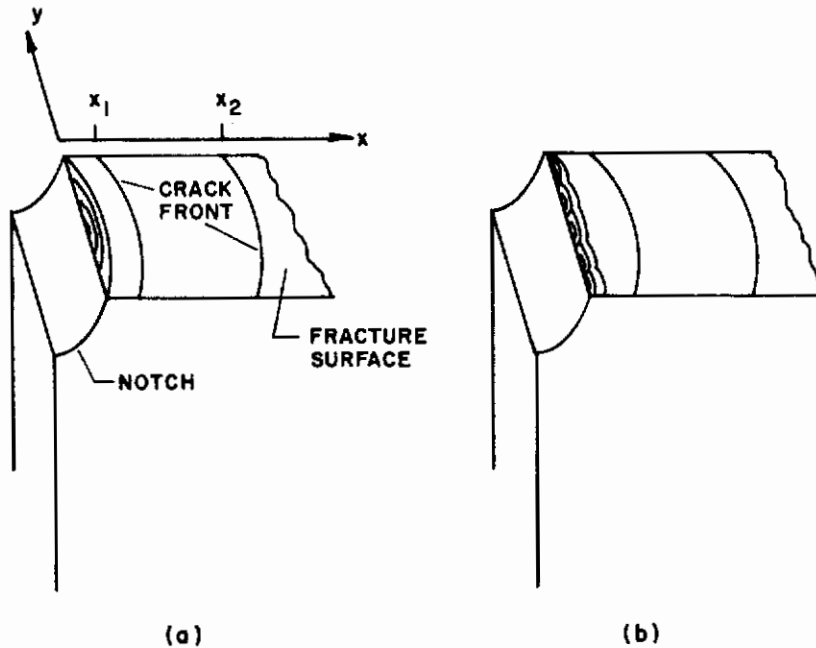


Figure 17 - Schematic Representation of Crack Front in 2024-T4 Fatigued at Low Stress (a), and High Stress (b). The x and y directions are defined in (a) and the position of the crack front at two different times is shown at x_1 and x_2 .

Contrails

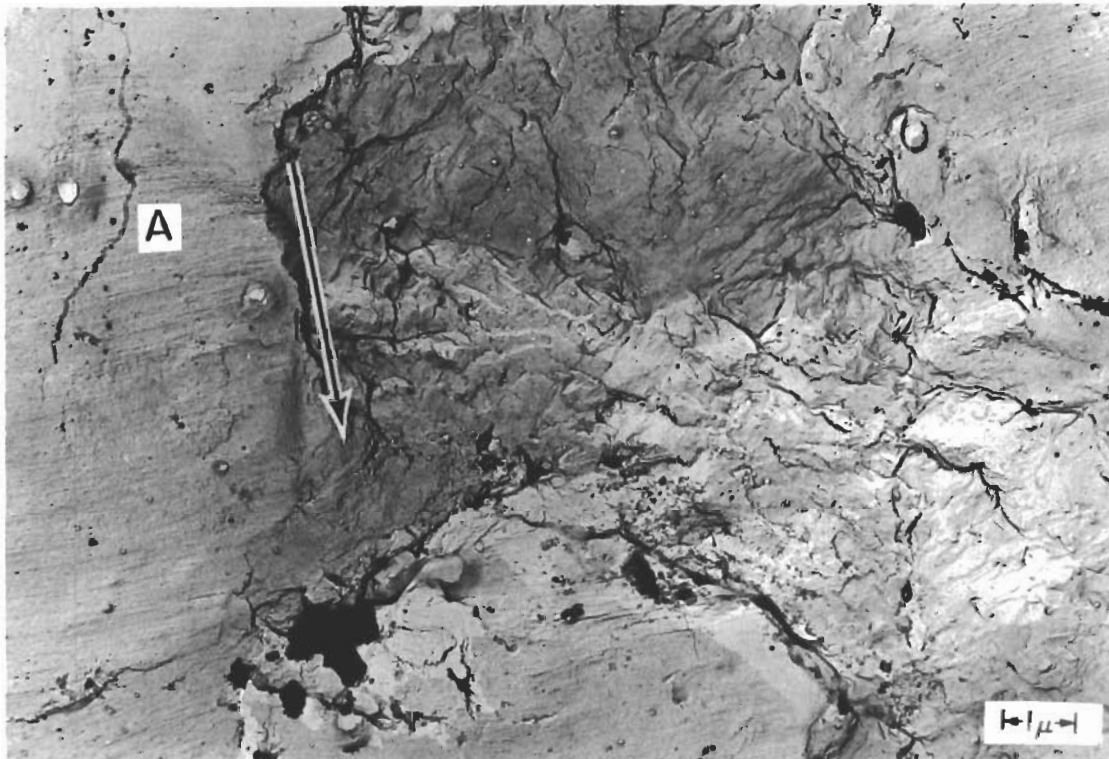
The nature of the crack propagation in the x direction can be inferred from fracture surface replicas. As in the case of 1100-0 aluminum, these replicas reveal a variety of crack growth mechanisms. Figure 18 illustrates some typical areas. In Figure 18(a) uniform striations which are found near the notch are probably associated with early propagation. Some of these striations are so straight and evenly spaced that they could as easily be interpreted as slip-line steps formed during extension of the crack. Figure 18(b) illustrates both an area of growth striations and a nondescript area in the center which probably fractured by a ductile tearing mechanism. Interesting features of this micrograph are the microcracks on the fracture face at the points marked A. These cracks probably developed at internal inclusions independently of the main fracture crack. A region of ductile-type fracture is shown in Figure 18(c). Some widely spaced growth striations can be seen in the lower right-hand corner. Cleavage type markings are visible on the surface shown in Figure 18(d). Figure 18(e) shows a featureless surface except for what may be crack-arrest lines at B. All of these micrographs convey the unmistakable impression that no one mechanism of crack growth can be used to characterize the fatigue of 2024-T4 aluminum, nor is the crack front continuous or the extension mechanism coherent along the front at any given time.

The amount of particulate debris produced on the crack surface was larger in the case of 2024 aluminum than for 1100; however, the nature of the particles was the same, i.e., aluminum and aluminum oxide.

Transmission electron micrographs were obtained in the same manner as for the 1100-0 specimens. Figure 19(a) shows a typical area in a control, or unstrained sample. The volume fraction of constituent particle inclusions is 3.1 per cent. In nearly every case, the constituent particle has acted as a source of dislocations, the generation probably occurring during the quench which follows solution heat treatment. In some cases, the particles act as dual Frank-Read sources, e.g., at A. Figure 19(b) shows several of these dual sources in an earlier stage of operation. In the background of both these pictures, a fine microstructure is seen which is probably due to GP zones. The dislocations adjacent to a fatigue crack appear as in Figure 19(c). There is a large density of dislocation loops and tangles, especially around constituent particles. No cell structure or embryonic cell boundaries were observed in this alloy. Thirty-seven hundred microns ahead of the crack the material is indistinguishable from the control specimen, Figure 19(d). Comparison of the constituent particles in Figures 19(a), (c) and (d) shows that in the latter figure the particles are predominantly elongated. This difference is due to the fact that the section viewed in Figure 19(d) was cut parallel to the rolling direction, while those in the first two figures were cut transverse to the rolling direction. Typical size of the constituent particles is 3,000 - 4,000 Å long and 600 - 900 Å in diameter.



(a)



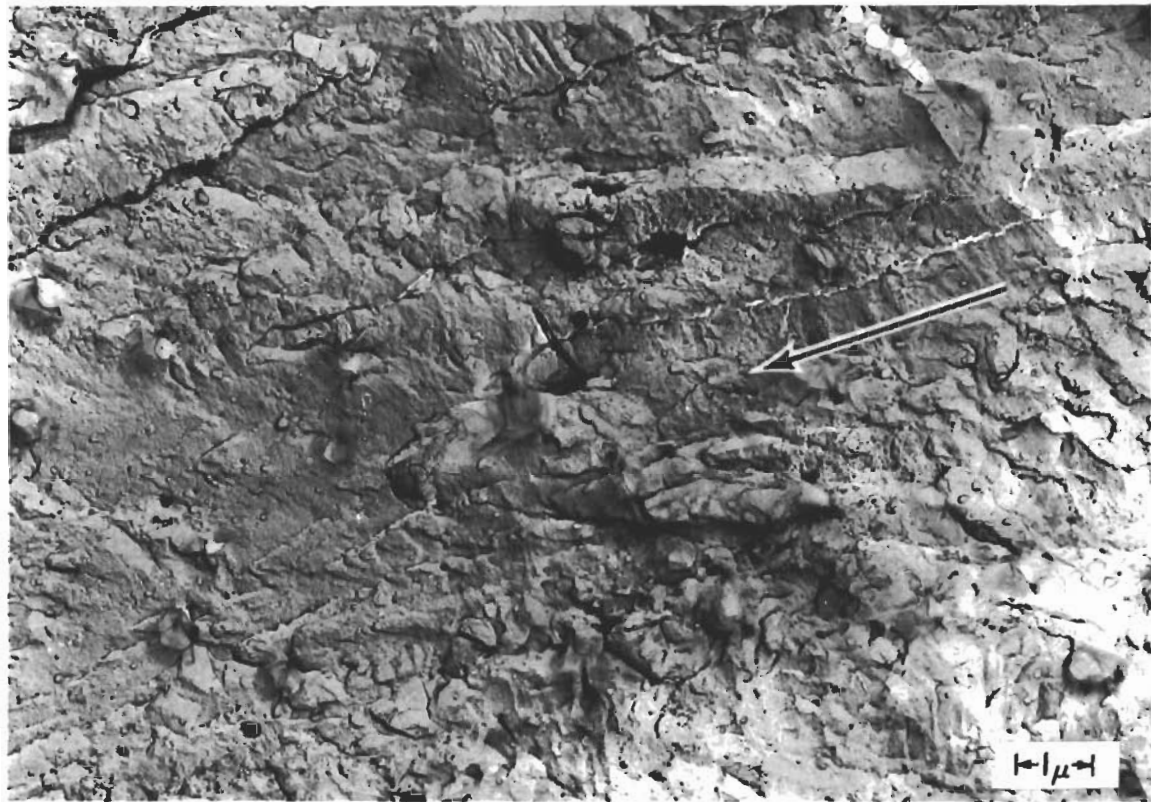
(b)

Figure 18 - Electron Micrographs of Typical Fracture Surface Area on 2024-T4 Aluminum. Crack growth (x-direction) indicated by arrows. (a) Uniform striations adjacent to notch. (b) Striations and ductile fracture areas. Notice microcracks at A. (c) Ductile fracture area. (d) Cleavage fracture area. (e) Featureless surface. Crack-arrest lines at B.

Contrails

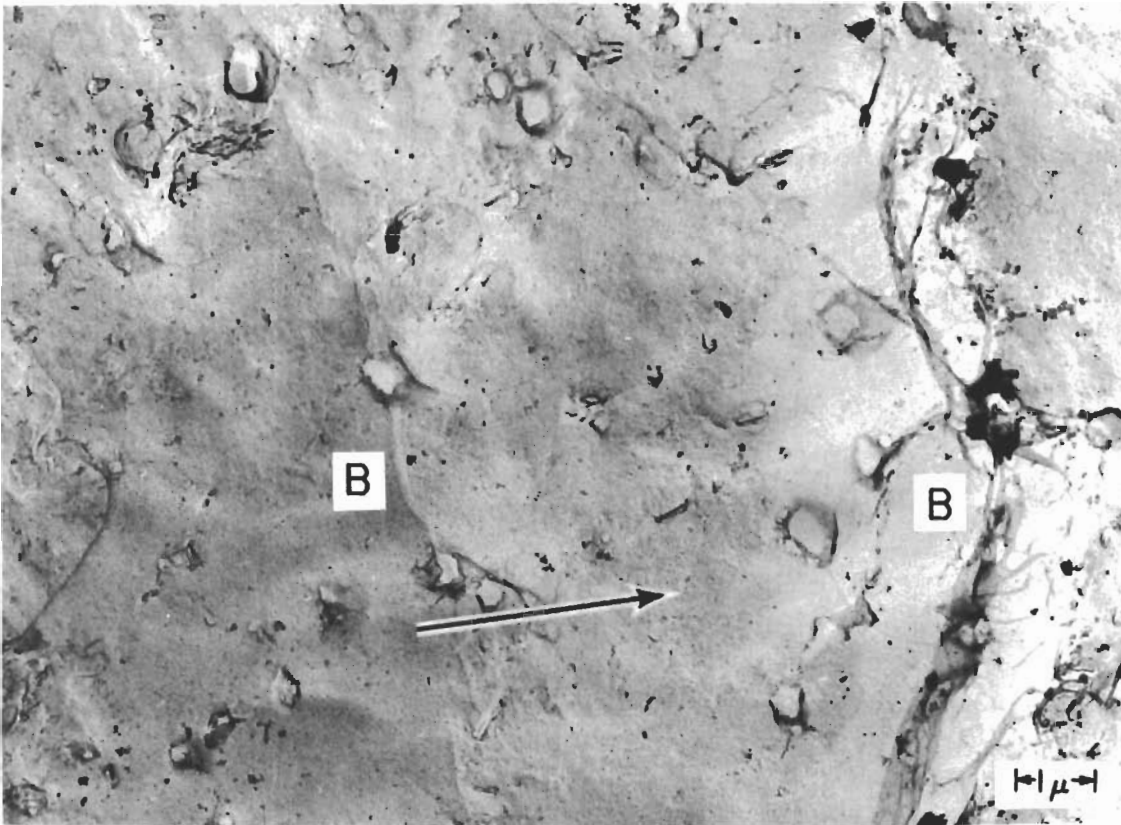


(c)



(d)

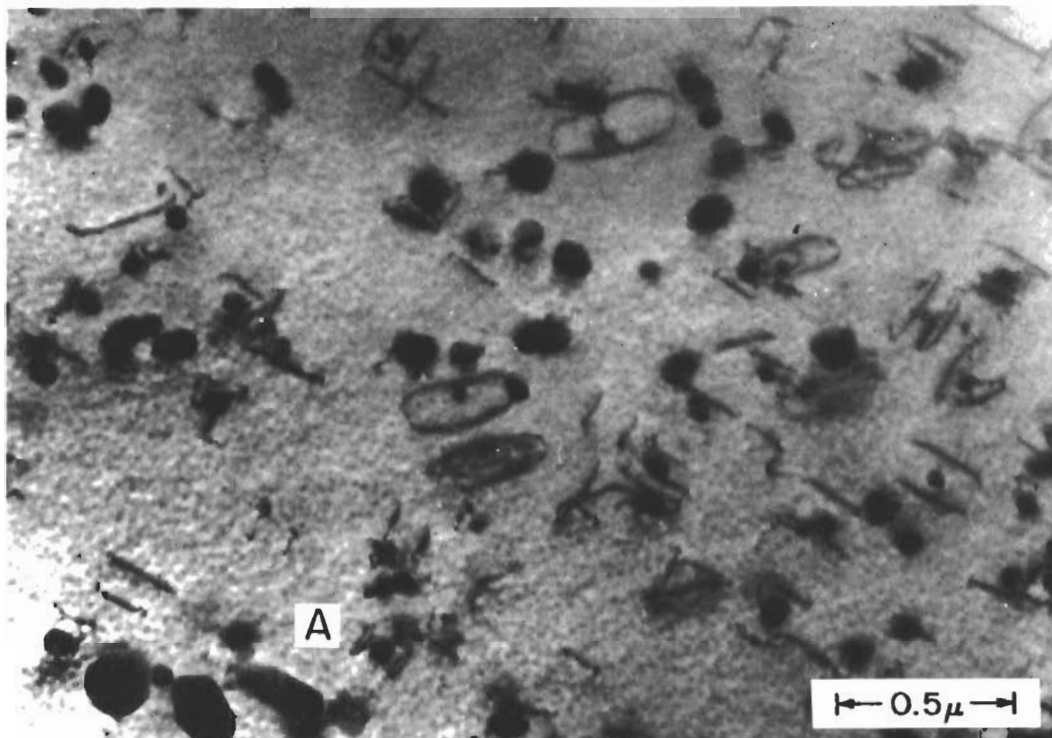
Figure 18 (Continued)



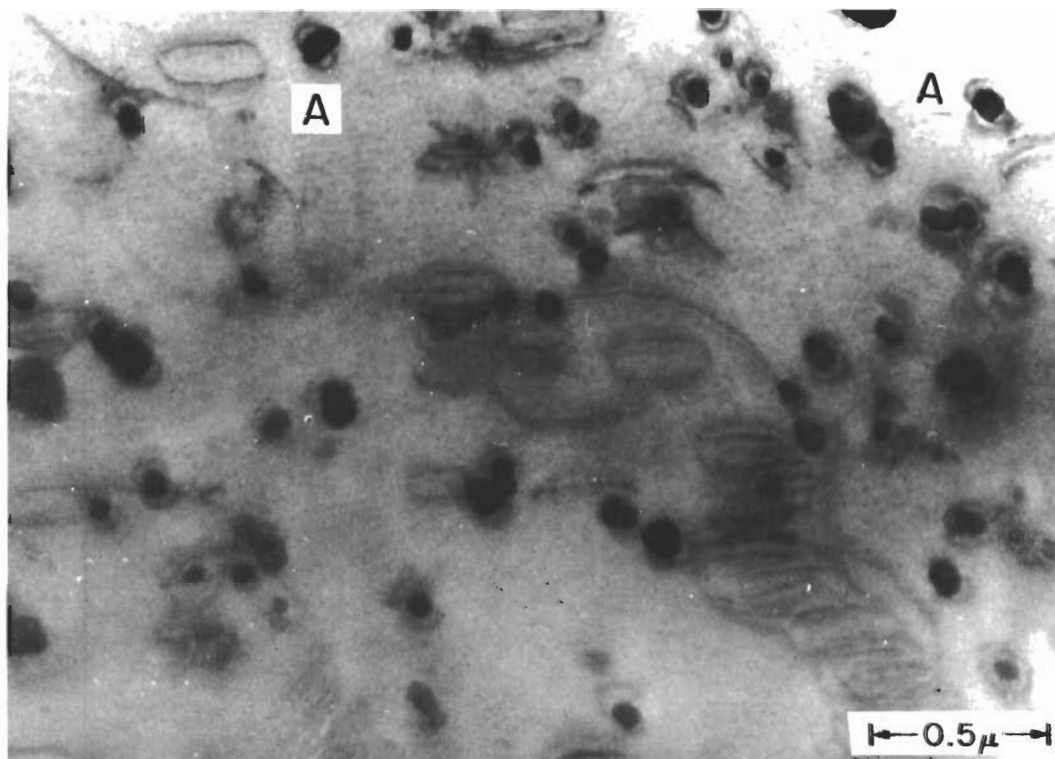
(e)

Figure 18 (Concluded)

Contrails



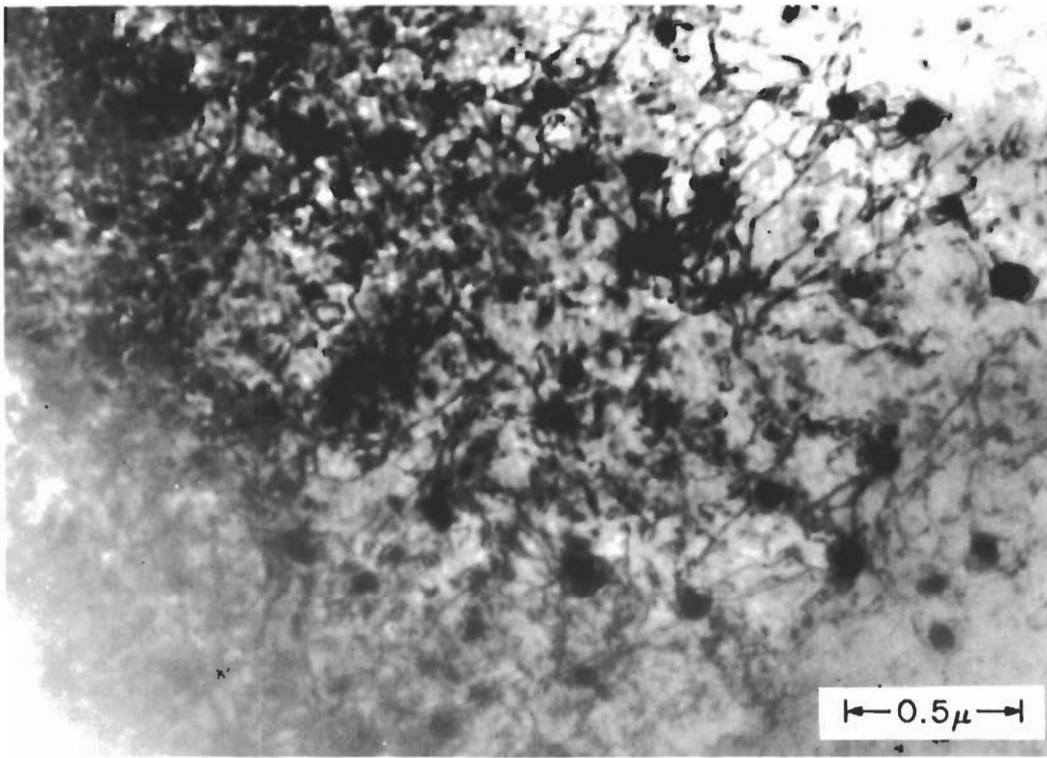
(a)



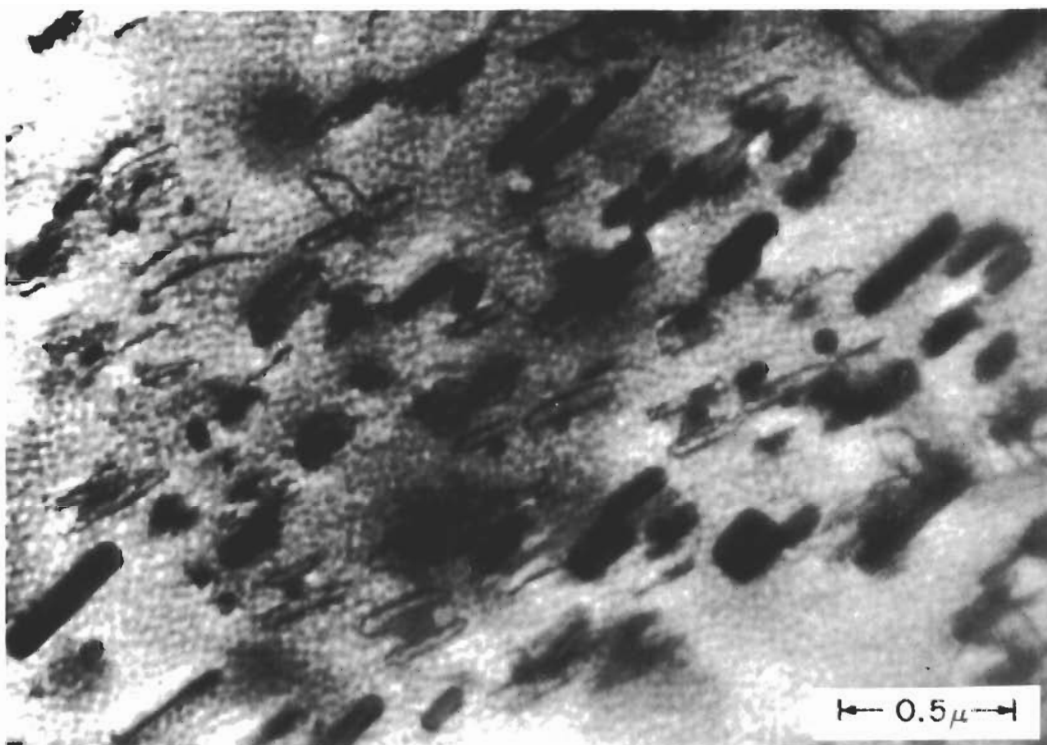
(b)

Figure 19 - Transmission Electron Micrographs of 2024-T4 Aluminum.
(a) Unstrained. Frank-Read source at A.
(b) Unstrained. Inclusions acting as dual F-R sources, A. (c) 6 Microns from fracture surface.
(d) 3,700 Microns ahead of crack-tip.

Contrails



(c)



(d)

Figure 19 (Concluded)

IV. DISCUSSION OF RESULTS

The mechanism of fatigue in 1100-0 aluminum is typical of the behavior of most pure metals. Fatigue cracks initiate at the surface in slip bands which begin deepening into fissures at the very beginning of fatigue life. Independent development of these fissures to a depth of 3 - 5 microns occupies 65 - 70 per cent of the total fatigue life. After this development, linkage of favorably oriented fissures into a single dominant crack occurs in a relatively short time. Complete failure occurs after the dominant crack advances across the bulk of the specimen. The growth rate of this crack is linearly proportional to the crack length. This mechanism and crack growth law are precisely the ones found earlier for 1100-0 aluminum single crystals (Refs. 6 and 7), for which a different specimen shape and method of loading were used.

Some of the details of this fatigue sequence in 1100-0 aluminum are clearer as a result of the present experiments. While our results do not allow us to distinguish between the several mechanisms proposed for slip-band fissure growth (Ref. 8), the measured rate of growth, 2×10^{-2} Å/cycle, does allow some conclusions concerning the mechanism. It is clear that fissure growth is intermittent, and that the dislocation motion necessary for extension of any one fissure occurs approximately every 100 cycles (Burger's vector for Al is 2.8 Å). Of course, dislocation motion and extension of a random set of fissures occur every cycle.

The definition one chooses for the crack nucleation period in 1100-0 aluminum is purely one of convenience. The deepening of certain slip bands into fissures probably begins after a brief rapid-hardening period of a few hundred cycles (Ref. 8), although our methods of observation prevent us from seeing this until $\sim 10^4$ cycles have elapsed. Nevertheless, cracks, in the strict sense of the word, are present from almost the beginning of the test. For the description of fatigue in terms of a continuous crack growth rate (Ref. 3), however, it is inconvenient to classify fissures as cracks. They grow at a rate different from the dominant crack, and then, there is the discontinuity in crack length which occurs when fissures link together. Moreover, the point in time at which linkage occurs cannot be accurately predicted. Thus, for the purposes of a unified crack growth theory, the term "crack nucleation" should include the entire period of independent fissure growth. As a compromise, we suggest that the word "crack" be always modified by the appropriate adjective, e.g., fissure crack, dominant crack, tensile-mode crack, etc. Then, the specification of crack nucleation and growth time becomes much easier and more specific.

Contrails

The mechanisms of dominant crack growth in 1100-0 aluminum consist of: (1) growth by repetitive extension and compression of the crack tip to form ripples or striations; (2) ductile tearing; and (3) brittle cleavage. Indications of all three mechanisms are found on surface micrographs of the fracture surface. Moreover, extension by ripple formation and by ductile tearing (or cleavage) may occur side by side. Of course, the simultaneity of operation of these mechanisms cannot be inferred from the fracture surfaces. A possible explanation for the heterogeneity of crack extension processes is shown in Figure 20.

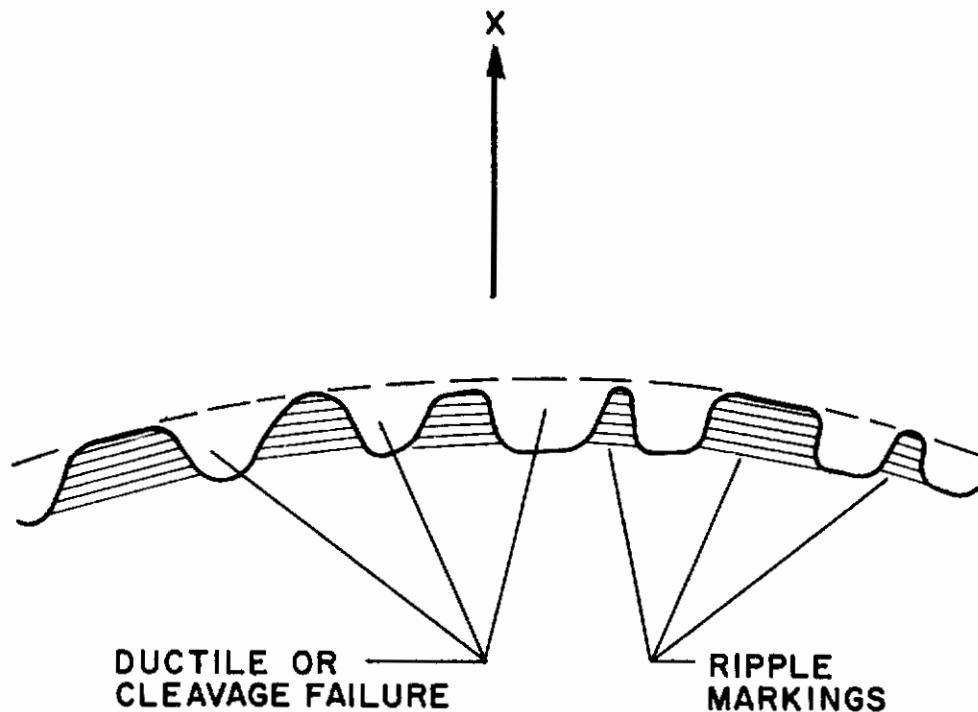


Figure 20 - Schematic Representation of Heterogeneous Crack Extension Mechanisms. Propagation is in the x-direction and the tensile axis is perpendicular to the plane of the paper.

Contrails

The basic process is supposed to be extension by repetitive tension and compression of the crack tip. It is assumed that such extension occurs along favorably oriented subgrain boundaries or within grains for which the available slip systems are favorably oriented for such extension. As shown in Figure 20, at any particular instant the crack front would consist of a series of bulges in which this extension has occurred. The intervening material will eventually fracture catastrophically either by ductile tearing or cleavage depending upon orientation and the availability of voids and inclusions which promote ductile fracture. The fact that the striation spacings observed on fracture surfaces of 1100-0 aluminum are usually larger than the crack growth rate observed on the face of the sample indicates that propagation by ripple formation does not occur simultaneously in all the little bulges along the crack front of Figure 20. Rather, one would expect that propagation occurs locally, but not continuously, along the entire crack front.

The transmission electron micrographs show clearly that in 1100-0 aluminum, as in high purity aluminum, large strain amplitudes result in the formation of a cell structure. Previous work (Ref. 4) has already shown that these cell boundaries are preferred paths of crack propagation. Because the formation of cells is essentially a strain relief mechanism, there is no reason to believe that any concentration of dislocations occurs ahead of the crack sufficient to cause the nucleation of internal voids. Propagation along subgrain boundaries is primarily a question of finding the path of least resistance. That is, less energy is required to produce new surface along the cell boundaries because of the stored energy available in the dislocation strain fields.

The mechanism of fatigue in 2024-T4 aluminum is heavily influenced by the presence of inclusions. At low stresses, a single crack pair nucleating at a surface inclusion propagates throughout at least 95 per cent of the life of the sample to cause complete failure. At higher stresses, the mechanism multiplies by nucleation of additional crack pairs which contribute to the early crack extension by linking with other such cracks. In a sense, this latter behavior is similar to the formation and linkage of many fissures to form the main crack in 1100-0 aluminum, although the mechanism and rate of fissure growth are different than those for inclusion crack-pair growth.

The nucleation of cracks at constituent particle inclusions is most likely the result of dislocation pile-up at the inclusions. A Stroh-type crack (Ref. 9) is formed whenever it becomes energetically favorable for the piled-up group to convert itself into a crack under the applied stress.

Under alternating stress, pile-ups will occur on both sides of an inclusion and give rise to the crack-pairs observed here. Lipsitt (Ref. 10) has used this same mechanism to explain the appearance of fatigue crack-pairs at

Contrails

impurity sites in nickel. McEvily and Boettner (Ref. 11), who observed fatigue crack nucleation at constituent particles in an Al-Zn-Mg-Cu alloy, report that the constituent particles themselves are cracked during fabrication and rolling, and that nucleation begins at these cracked particles. On the present work, we were unable to rule out this possibility entirely because of artifacts which formed during replication of the unstrained samples.

The crack nucleation period in 2024-T4 aluminum can be defined as the time required to form a Stroh crack-pair at an inclusion. From the present work, this period is less than 5 per cent of the total fatigue life. In all likelihood, patient electron microscopy of the notch surface replicas could establish this period at a still smaller fraction of total life.

The growth of a crack-pair across the face of the notch occurs essentially under conditions of plane stress, since the crack is never very deep at this stage. The observed growth rates, proportional to the fourth power of the stress intensity factor, $\sigma\sqrt{l}$, are consistent with other results obtained for the structural aluminum alloys under plane stress conditions (Ref. 3).

Fracture surface patterns adjacent to the notch suggest that the microcracks can grow by either a ripple mechanism or by more complex ductile and cleavage mechanisms. In fact, the analysis of fractographs of 2024-T4 yields essentially the same conclusions as those reached for 1100-O aluminum, namely, that crack extension is heterogeneous and consists of at least three mechanisms which operate independently and noncoherently along the crack front. Moreover, the large volume fraction of inclusions in the 2024-T4 alloy further complicates the situation by providing barriers to arrest the crack (Figure 18(e)) or to assist in ductile or cleavage fracture.

The deformation at the crack tip as revealed by transmission electron micrograph is primarily one of limited dislocation motion due to the presence of inclusion particles. The mean free path of dislocations is too small to allow the formation of cell structure, and it is only when the stress concentration at the crack tip becomes quite large (Figure 13) that multiple slip can occur to produce visible slip bands on the surface of the samples. The large concentration of dislocation loops at the crack tip indicates that considerable to-and-fro motion of jogged screw dislocations has occurred. Due to the lack of a strain release mechanism, such as cell formation, and the barrier action of the constituent particle inclusions, it is entirely possible that stress concentrations can build up ahead of the crack tip sufficient to cause internal cracking. Several examples of this have been observed on the fracture surfaces, e.g., Figure 18(d).

Recently, Clark and McEvily (Ref. 12) have shown that an aluminum-4 per cent copper alloy undergoes reversion during cyclic straining and they

proposed that the softening which thus occurs can account for the low fatigue strength of the age-hardened aluminum alloy systems. A careful examination of Figure 19(a) and (c) shows that the background of GP zone structure visible in Figure 19(a) is not as prominent after fatigue in Figure 19(c), which would indicate that some reversion had taken place. A complicating factor is the presence of an anodic layer on the surface of these thin foils which has a microstructure whose dimension is of the same order as the metallurgical GP zone structure of the alloy. Further experiments are therefore necessary before one could safely conclude whether reversion occurs in commercial 2024-T4 aluminum during cyclic straining.

The differences in fatigue mechanisms observed for 1100-0 and 2024-T4 aluminum are due primarily to the impurity content and precipitate structure of the latter. For super-purity aluminum alloys, fatigue cracks have been observed to nucleate in surface slip bands (Ref. 13) so that an obvious effect of the constituent particles in commercial 2024-T4 has been to alter the mechanism of crack nucleation. While the mechanisms of crack growth, as inferred from fractographic studies, are essentially the same in the 1100-0 and 2024-T4 specimens, the dependence of crack growth rate on $\sigma\sqrt{l}$ is considerably different. The clue to this difference in behavior is obtained from the dislocation structures observed at the crack tips. The strain relief afforded by cell formation in 1100-0 aluminum acts as an energy sink so that crack growth depends only on the square of $\sigma\sqrt{l}$. (At higher net-section stresses, general energy dissipation in plastic deformation further lowers the exponent to ~ 0.75 .) In 2024-T4 aluminum, the crack tip deformation is restricted by inclusions and metallurgical structure (GP zones) so that considerable strain energy is stored in the lattice, internal cracking may occur (Figure 18(b)), and the crack growth now depends on the fourth power of $\sigma\sqrt{l}$.

The heterogeneous mixture of crack growth mechanisms which have been observed in both materials leads one to ask whether it will ever be possible to construct a reasonable theory of crack growth, or whether crack growth rates observed on the surface have any relation to a fundamental mechanism of crack extension. These are valid questions, and the answers do not come readily. Clearly, over-all extension of a crack front from x_1 to x_2 (Figure 17) involves averaging over a large number of local extensions by different mechanisms. Perhaps a statistical approach to the theory of crack growth offers the best solution to the questions which have been raised by the present observations.

The results reported here should also serve as a warning against generalizing a fatigue mechanism which is observed on only one particular type of specimen. It should be clear that the mechanism of fatigue depends strongly on the purity of the material, the presence of constituent particle inclusions and the stability of the precipitate structure.

V. CONCLUSIONS

The conclusions to be drawn from these experiments can be listed briefly as follows:

1. Fatigue cracks nucleate in slip bands on the surface of 1100-0 aluminum. Nucleation of slip-band fissures requires less than 0.5 per cent of the total fatigue life.
2. Slip-band fissure cracks on 1100-0 aluminum, which grow in depth at the average rate of 2×10^{-2} Å/cycle, link into a dominant crack across the surface of a notch at approximately 65 - 70 per cent of total fatigue life.
3. The growth rate of the final, dominant crack in 1100-0 aluminum is proportional to the second power of the stress intensity factor, $\sigma \sqrt{l}$, for $\sigma < \sigma_y$, and to the $3/4$ power when $\sigma > \sigma_y$.
4. Fatigue cracks nucleate in pairs at constituent particle inclusions on the surface of 2024-T4 aluminum. Nucleation of these crack pairs requires less than 5 per cent of the total fatigue life.
5. At low stresses, a single crack-pair grows completely across the surface of a notch in 2024-T4 aluminum in approximately 90 per cent of total fatigue life. The growth rate is proportional to the fourth power of $\sigma \sqrt{l}$.
6. At high stresses, many crack-pairs nucleate on the surface of a notch in 2024-T4 aluminum and link together to form a dominant crack across the notch at approximately 50 per cent of total fatigue life. The growth rate of any one crack pair is proportional to the fourth power of $\sigma \sqrt{l}$.
7. The difference in crack growth rate dependence on $\sigma \sqrt{l}$ for 1100-0 and 2024-T4 aluminum is interpreted as being due to the different mode of plastic deformation observed at the fatigue crack tips. Cell structure forms by a strain relief mechanism in 1100-0, while inclusions and GP zones restrict dislocation motion to loop and tangle formation on 2024-T4. Evidence for internal cracking ahead of the main crack in 2024-T4 is presented also.
8. Crack extension is observed to occur in both 1100-0 and 2024-T4 aluminum by a heterogeneous mixture of ripple formation, ductile, and cleavage fracture, which occurs noncoherently at local regions along the crack front.

REFERENCES

1. J. C. Grosskreutz, "A Critical Review of Micromechanisms in Fatigue," Fatigue - An Interdisciplinary Approach, p. 27, Syracuse University Press (1964).
2. G. Shaw and M. T. Lavik, Electron Microscopy, pp. FF-10, Academic Press (1962).
3. P. Paris and F. Erdogan, Trans. ASME, J. of Basic Engineering, 85, 528 (1963).
4. J. C. Grosskreutz, "Research on the Mechanisms of Fatigue," WADD TR-60-313, Part II, December 1963.
5. J. C. Grosskreutz and P. Waldow, Acta Metallurgica, 11, 717 (1963).
6. J. C. Grosskreutz, J. Appl. Phys., 33, 1787 (1962).
7. J. C. Grosskreutz, WADD TR-60-313, April 1960.
8. D. H. Avery and W. A. Backofen, "Nucleation and Growth of Fatigue Cracks," Fracture of Solids, p. 339, Interscience (1963).
9. A. N. Stroh, Adv. in Physics, 6, 418 (1957).
10. H. A. Lipsitt, "Crack Propagation in Cumulative Damage Fatigue Tests," Proc. of 11th Air Force Science and Engineering Symposium (1964).
11. A. J. McEvily and R. C. Boettner, Fracture of Solids, p. 383, Interscience (1963).
12. J. B. Clark and A. J. McEvily, Acta Metallurgica, 12, 1359 (1964).
13. P. J. E. Forsyth, Acta Metallurgica, 11, 703 (1963).

Contrails

UNCLASSIFIED

Security Classification

DOCUMENT CONTROL DATA - R&D		
(Security classification of title, body of abstract and indexing annotation must be entered when the overall report is classified)		
1 ORIGINATING ACTIVITY (Corporate author) Midwest Research Institute 425 Volker Boulevard Kansas City, Missouri 64110	2a. REPORT SECURITY CLASSIFICATION Unclassified	
	2b. GROUP N/A	
3. REPORT TITLE Mechanisms of Fatigue in 1100-0 and 2024-T4 Aluminum		
4. DESCRIPTIVE NOTES (Type of report and inclusive dates) Final Report - 1 April 1964 to 31 March 1965		
5. AUTHOR(S) (Last name, first name, initial) Grosskreutz, J. C. Shaw, G. G.		
6. REPORT DATE July 1965	7a. TOTAL NO. OF PAGES 37	7b. NO. OF REFS 13
8a. CONTRACT OR GRANT NO. AF 33(657)-10883 b. PROJECT NO. 7353 c. Task No. 735301 d.	9a. ORIGINATOR'S REPORT NUMBER(S) AFML-TR-65-127	
	9b. OTHER REPORT NO(S) (Any other numbers that may be assigned this report) None	
10. AVAILABILITY/LIMITATION NOTICES Qualified users may obtain copies of this report from the Defense Documentation Center (DDC), Alexandria, Va. The distribution of this report is limited because it contains technology identifiable with items on the Mutual Defense Assistance Control List excluded from export under U.S. Export Control Act of 1949, as implemented by AFR 400-10.		
11. SUPPLEMENTARY NOTES N/A	12. SPONSORING MILITARY ACTIVITY Metals and Ceramics Division Air Force Materials Laboratory Wright-Patterson AFB, Ohio 45433	
13. ABSTRACT The mechanisms of fatigue in notched 1100-0 and 2024-T4 aluminum have been studied by means of optical and electron microscopy. It was found that fatigue cracks nucleated at slip bands on the surface of 1100-0 aluminum in less than 0.5 per cent of total fatigue life. These slip-band fissure cracks grew independently for 65 - 70 per cent of life and then linked rather quickly into a dominant crack which accounted for final failure. The crack growth rates were recorded for both fissure and dominant cracks. On the surface of 2024-T4 aluminum, cracks nucleated in pairs at constituent particle inclusions in less than 5 per cent of total fatigue life. At low stresses, a single crack-pair grew across the notch in about 90 per cent of life and accounted for complete failure as it continued across the sample face. At high stresses, many crack-pairs were nucleated in the notch, some of which linked to form a dominant crack at ~ 50 per cent of life. The difference in crack growth rate dependence on $\sigma \sqrt{a}$, observed for 1100-0 and 2024-T4 aluminum, is discussed in terms of the different dislocation distributions observed at the crack tips. Crack extension in both 1100-0 and 2024-T4 aluminum was observed to occur by a heterogeneous mixture of ripple formation, ductile and cleavage fracture which occurs noncoherently at local regions along the crack front. Some of the consequences of this observation for crack propagation theories are discussed.		

DD FORM 1 JAN 64 **1473**

0101-807-6800

UNCLASSIFIED

Security Classification

14	KEY WORDS	LINK A		LINK B		LINK C	
		ROLE	WT	ROLE	WT	ROLE	WT
	1100-0 Aluminum 2024-T4 Aluminum Fatigue Mechanisms Fatigue Fractography Inclusions Crack Propagation						

INSTRUCTIONS

1. **ORIGINATING ACTIVITY:** Enter the name and address of the contractor, subcontractor, grantee, Department of Defense activity or other organization (*corporate author*) issuing the report.
- 2a. **REPORT SECURITY CLASSIFICATION:** Enter the overall security classification of the report. Indicate whether "Restricted Data" is included. Marking is to be in accordance with appropriate security regulations.
- 2b. **GROUP:** Automatic downgrading is specified in DoD Directive 5200.10 and Armed Forces Industrial Manual. Enter the group number. Also, when applicable, show that optional markings have been used for Group 3 and Group 4 as authorized.
3. **REPORT TITLE:** Enter the complete report title in all capital letters. Titles in all cases should be unclassified. If a meaningful title cannot be selected without classification, show title classification in all capitals in parenthesis immediately following the title.
4. **DESCRIPTIVE NOTES:** If appropriate, enter the type of report, e.g., interim, progress, summary, annual, or final. Give the inclusive dates when a specific reporting period is covered.
5. **AUTHOR(S):** Enter the name(s) of author(s) as shown on or in the report. Enter last name, first name, middle initial. If military, show rank and branch of service. The name of the principal author is an absolute minimum requirement.
6. **REPORT DATE:** Enter the date of the report as day, month, year, or month, year. If more than one date appears on the report, use date of publication.
- 7a. **TOTAL NUMBER OF PAGES:** The total page count should follow normal pagination procedures, i.e., enter the number of pages containing information.
- 7b. **NUMBER OF REFERENCES:** Enter the total number of references cited in the report.
- 8a. **CONTRACT OR GRANT NUMBER:** If appropriate, enter the applicable number of the contract or grant under which the report was written.
- 8b, 8c, & 8d. **PROJECT NUMBER:** Enter the appropriate military department identification, such as project number, subproject number, system numbers, task number, etc.
- 9a. **ORIGINATOR'S REPORT NUMBER(S):** Enter the official report number by which the document will be identified and controlled by the originating activity. This number must be unique to this report.
- 9b. **OTHER REPORT NUMBER(S):** If the report has been assigned any other report numbers (*either by the originator or by the sponsor*), also enter this number(s).
10. **AVAILABILITY/LIMITATION NOTICES:** Enter any limitations on further dissemination of the report, other than those

imposed by security classification, using standard statements such as:

- (1) "Qualified requesters may obtain copies of this report from DDC."
- (2) "Foreign announcement and dissemination of this report by DDC is not authorized."
- (3) "U. S. Government agencies may obtain copies of this report directly from DDC. Other qualified DDC users shall request through _____."
- (4) "U. S. military agencies may obtain copies of this report directly from DDC. Other qualified users shall request through _____."
- (5) "All distribution of this report is controlled. Qualified DDC users shall request through _____."

If the report has been furnished to the Office of Technical Services, Department of Commerce, for sale to the public, indicate this fact and enter the price, if known.

11. **SUPPLEMENTARY NOTES:** Use for additional explanatory notes.

12. **SPONSORING MILITARY ACTIVITY:** Enter the name of the departmental project office or laboratory sponsoring (*paying for*) the research and development. Include address.

13. **ABSTRACT:** Enter an abstract giving a brief and factual summary of the document indicative of the report, even though it may also appear elsewhere in the body of the technical report. If additional space is required, a continuation sheet shall be attached.

It is highly desirable that the abstract of classified reports be unclassified. Each paragraph of the abstract shall end with an indication of the military security classification of the information in the paragraph, represented as (TS), (S), (C), or (U).

There is no limitation on the length of the abstract. However, the suggested length is from 150 to 225 words.

14. **KEY WORDS:** Key words are technically meaningful terms or short phrases that characterize a report and may be used as index entries for cataloging the report. Key words must be selected so that no security classification is required. Identifiers, such as equipment model designation, trade name, military project code name, geographic location, may be used as key words but will be followed by an indication of technical context. The assignment of links, roles, and weights is optional.